Comparison of Heat Exchanger Designs for Aircraft Thermal Management

William Cody Reed

Thesis submitted to the Faculty of the

Virginia Polytechnic Institute and State University

in partial fulfillment of the requirements for the degree of

Master of Science

In

Aerospace Engineering

Pradeep Raj, Co- Chair

Michael R. von Spakovsky, Co- Chair

Seongim Choi

May 5, 2015

Blacksburg, Virginia

Keywords: Thermal Management System, Optimization, Aerospace, Heat Exchangers, Thermal Storage

Comparison of Heat Exchanger Designs for Aircraft Thermal Management

William Cody Reed

Thermal management has become a major concern in the design of current and future more and all electric aircraft (M/AEA). With ever increasing numbers of on-board heat sources, higher heat loads, limited and even decreasing numbers of heat sinks, integration of advanced intelligence, surveillance and reconnaissance (ISR) and directed energy weapons, requirements for survivability, the use of composite materials, etc., existing thermal management systems and their components have been pushed to the limit. To address this issue, more efficient methods of thermal management must be implemented to ensure that these new M/AEA aircraft do not overheat and prematurely abort their missions. Crucial to this effort is the need to consider advanced heat exchanger concepts, comparing their designs and performance with those of the conventional compact exchangers currently used on-board aircraft thermal management systems. As a step in this direction, the work presented in this thesis identifies two promising advanced heat exchanger concepts, namely, microchannel and phase change heat exchangers. Detailed conceptual design and performance models for these as well as for a conventional plate-fin compact heat exchanger are developed and their design and performance optimized relative to the criterion of minimum dry weight. Results for these optimizations are presented, comparisons made, conclusions drawn, and recommendations made for future research. These results and comparisons show potential performance benefits for aircraft thermal management incorporating microchannel and phase change heat exchangers.

Acknowledgements

This thesis would not have been possible without the assistance of many people. I would like to thank both of my advisors, Dr. Pradeep Raj and Dr. Michael von Spakovsky, for giving me the opportunity to work on this project and providing me with guidance and pushing me to do better throughout the entire process. Without you this work would not exist. I would also like to thank Dr. Seongim Choi for serving on my committee and providing assistance when needed.

To all of the friends I have made in Blacksburg, thanks for helping in so many ways to allow this work to be completed. Special thanks to the other aerospace graduate students that listened to my ideas and provided distractions when I needed to get away for a while.

To Megan, thank you for supporting me through this past year. You always kept me going even while being away and provided a bright spot in many long days.

To my parents, Dana and Cathy, and my sister, Molly, I cannot give enough thanks. Your unwavering support and love has allowed me to accomplish all that I have. Without you, I could've completed only a small piece of what was done. This work is dedicated to you.

Table of Contents

List of Figures

List of Tables

Nomenclature

MEA	More Electric Aircraft
DEW	Directed Energy Weapon
TMS	Thermal Management Subsystem
PCES	Phase Change Energy Storage
MDO	Multidisciplinary Design Optimization
AVS	Aircraft Vehicle Subsystem
APTMS	Adaptive Power and Thermal Management Subsystem
REPS	Robust Electrical Power Subsystem
PS	Propulsion Subsystem
FTMS	Fuel Thermal Management Subsystem
PCM	Phase Change Material
HPEAS	High Power Electrical Actuation Subsystem
PAO	Polyalphaolefin
TES	Thermal Energy Storage
NTU	Number of Transfer Units

Chapter 1 - Introduction

Rapid advancements in advanced aircraft avionics and weapons technologies have prompted designers to integrate these new technologies into current and future aircraft for enhanced performance. These technologies, which include items such as advanced sensors, electrical actuators, directed energy weapons, and glass cockpit avionics have caused a significant increase in the thermal and power loads that an aircraft must be able to handle and this trend of increasing thermal loads is projected to increase into the future[1]. With this increasing trend in power and thermal loads, it is becoming more and more critical that these loads be addressed early in the design process so that costly redesigns of other systems can be avoided.

1.1 Historical Background

1.1.1 More Electric Aircraft

The research being conducted by the Air Force Research Lab (AFRL) and others[1, 2] shows that aircraft are including more and more electrical systems and components, therefore becoming what has been termed the more electric aircraft (MEA). In older aircraft, the power needed for several key aircraft systems is derived mainly from mechanical means such as pneumatic or hydraulic systems. In a MEA, such systems are being increasingly replaced by engine driven generators that power electrical systems performing the same functions previously done by the mechanical systems. These functions include such things as cabin pressurization, air conditioning, landing gear actuation, and others[2].

There are several reasons behind the progression toward the MEA. With the removal of the mechanical power systems there is a possibility for a reduction in system weight as well as improved engine efficiency due to the fact that less of the power used for thrust has to be extracted with the replacement electrical systems. This is because the electrical generators, actuators, and other components used in MEA are more efficient than the older mechanical systems. Other benefits of using electrical over mechanical systems is the fact that they only need to be powered on demand, can allow for more intelligent maintenance, and therefore, result in increased aircraft availability. All of these benefits factored together could lead to aircraft with reduced operating costs, reduced fuel burn, and reduced environmental impact[2]. Of course, issues of reliability and thermal management temper this assessment since for example more electric

loads lead to higher thermal loads and the possibility of larger thermal systems or a curtailment of mission ranges or capabilities. The issue of mechanical systems versus electrical system reliability is also an open question.

On top of the electrical systems mentioned above there has also been a change in the usage of advanced sensors and directed energy weapons in military aircraft. Advances in radar and other sensing technology has created sensors with even larger heat loads and power needs then previous systems. Also, the advent of directed energy systems has created another issue with which aircraft thermal management systems must contend. These weapon systems can produce significant localized heat loads as well as extremely high peak loads that current thermal management systems are not designed to handle.

1.1.2 Directed Energy

Directed energy devices are increasingly being looked at as weapons systems for military applications. These devices have recently been proven to be effective in both offensive and defensive roles in a multitude of environments. Previous efforts in directed energy research have included such programs as the Airborne Laser (ABL), Advanced Tactical Laser (ATL), Joint High-Power Solid State Laser (JHPSSL), and others[3]. These efforts have shown that directed energy technology still needs to mature before it can successfully be used in weapons systems. However, with recent developments, the point of maturity is getting closer and closer.

Directed energy weapons work by depositing energy onto a target. This can be done in a multiple of ways including microwaves, acoustic waves, particle waves, or lasers. Lasers in particular have been a point of interest for application in weapons systems for some time. A laser works by having an energy source charge an atomic system. This causes electrons to move from lower to higher energy states, storing the input energy. When an electromagnetic wave of the appropriate wavelength is applied, this charged atomic system releases photons at a similar wavelength and drops the electrons back down to a lower energy state. These photons are then directed through optical equipment to form a powerful beam of energy[4].

1.2 Problem Description

1.2.1 Thermal Issues in Modern Aircraft

As discussed in Section 1.1, there are many factors contributing to an increased heat load from an aircraft's systems. Increased electrical demands from advanced avionics and the use of more electrical versus mechanically driven systems have worked to greatly increase the thermal strain on modern aircraft. This increase in heat load must be successfully managed to ensure that an aircraft is able to complete its mission. In order to manage these heat loads, aircraft incorporate a thermal management subsystem (TMS). This system works to remove heat from heat sources and either move it to heat sinks or expel it from the aircraft all together.

With the rapid increase of the thermal requirements, thermal management is becoming more and more important. As seen in Figure 1.1, the thermal requirements of military aircraft have steadily increased over the past couple of decades and are expected to continue to increase into the future.

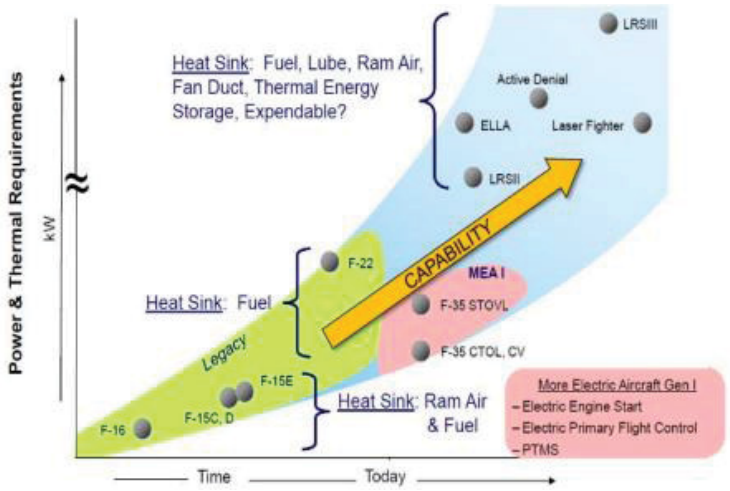

Figure 1.1 Aircraft thermal requirements over time. von Spakovsky, M.R. "Mission and Aircraft level Thermal Management System Research Overview". In Aerospace Systems &Technology Conference. 2014. Cincinnati, OH.[a]

Complicating the issue of increased heat loads is the fact that modern aircraft also have decreasing heat storage and rejection capabilities[1]. This is due to several reasons. One of these is the fact that modern aircraft carry less onboard fuel due to greater fuel efficiencies.

[a] Figure 1.1 is taken from material that is a work of the U.S. Government and not subject to copyright protection in the United States

Fuel traditionally has been used as one of the main heat sinks for excess aircraft heat loads. By carrying less fuel, an aircraft has a diminished ability to store its excess heat. Another reason is the increase in the usage of composite materials in aircraft structures. These composite structures reduce the ability to reject heat from the aircraft through its structure by reducing the amount of conductive cooling that can be completed through the aircraft's skin. These factors combine to make the already growing problem of increasing heat loads even more difficult to control.

On top of the increase in heat loads due to the movement towards the MEA, directed energy weapons (DEWs) complicate the thermal management problem even further. DEWs generate large, localized heat loads that must be taken into account when designing a TMS[4]. A typical DEW has an operating efficiency of between 10% to 25%. This means that a solid state laser meant to output 100 kW of power releases as much as 526 kW of heat load. This is a very large amount of energy that is almost an order of magnitude higher than the typical peak heat loads seen in current high performance aircraft.

In order to combat the heat loads generated onboard an aircraft, a TMS must be designed to take heat away from heat sources and transfer it either to a heat sink for storage or eject if off board the aircraft to the atmosphere. Conventional TMSs utilize a number of working fluids such as fuel, air, and oil to move the heat through a series of heat exchangers. These fluids pick up sensible heat from thermal loads and move it either to a heat sink such as the fuel tank or eject it into the atmosphere. If the thermal load on the system is too high, the system is not be able to keep up with the load placed on it, causing an increase in the temperatures of the avionics, fuel cabin, etc. with the consequence of system failure or mission curtailment.

1.2.2 Simulation of a Mission

In order to get a representation of the heat loads with which an advanced aircraft TMS would need to deal, a mission is simulated by Gvozdich[4] and Weise[5] using a tip-to-tail aircraft model. From this simulation, representative heat loads on the various parts of an overall TMS onboard are calculated. These values are then used to design individual components of the TMS consistent up to the aircraft and mission levels. Figure 1.2 and Table 1.1 give details of the mission profile used for the mission simulation and the component optimizations. It is those heat loads that are used in this thesis research as the basis for the heat exchanger and phase change energy storage device design optimization studies.

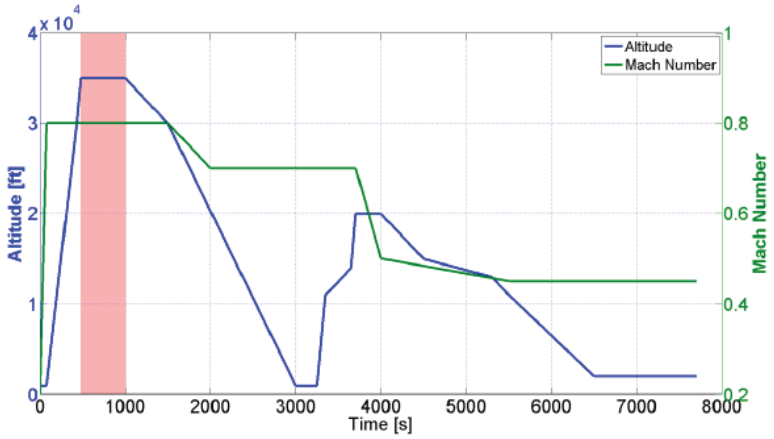

Figure 1.2 Tip-to-tail mission profile. Gvozdich, G., "Modeling the Effects of Transient High Energy Weapon Subsystems on High-performance Aerospace Systems, in Mechanical Engineering". 2011, M.S. thesis advisor: M.R. von Spakovsky, ME dept., Virginia Tech Blacksburg, VA. Used with Permission of Grant Gvozdich, 2015

Table 1.1 Tip-to-tail mission profile in detail. Gvozdich, G., "Modeling the Effects of Transient High Energy Weapon Subsystems on High-performance Aerospace Systems, in Mechanical Engineering". 2011, M.S. thesis advisor: M.R. von Spakovsky, ME dept., Virginia Tech Blacksburg, VA. Used with Permission of Grant Gvozdich, 2015

Mission Segment	Description	Duration [s]	Starting Speed [Ma]	Ending Speed [Ma]	Starting Altitude [ft]	Ending Altitude [ft]
1	Subsonic Acceleration	78	0	0.8	1,000	1,000
2	Transonic Climb	405	0.8	0.8	1,000	35,000
3	Transonic Cruise	517	0.8	0.8	35,000	35,000
4	Transonic Descent	500	0.8	0.8	35,000	30,000
5	Subsonic Deceleration/ Descent 1	500	0.8	0.7	30,000	20,333
6	Subsonic Descent 1	1000	0.7	0.7	20,333	1,000
7	Subsonic Cruise 1	250	0.7	0.7	1,000	1,000
8	Subsonic Climb	454	0.7	0.7	1,000	20,000
9	Subsonic Deceleration	296	0.7	0.5	20,000	20,000
10	Subsonic Deceleration / Descent 2	1500	0.5	0.45	20,000	11,000
11	Subsonic Descent 2	1200	0.45	0.45	11,000	2,000
12	Subsonic Cruise 2	1000	0.45	0.45	2,000	2,000

1.3 Thesis Objectives

The purpose of this research is to investigate the benefits of using advanced heat exchanger technology to combat the growing heat loads generated by more electric aircraft and directed energy weapons systems. These benefits are investigated by modeling, simulating, and analyzing a microchannel heat exchanger, a plate fin compact heat exchanger, and a thermal energy storage system to see where these technologies can be used to improve current TMSs.

The first objective is to develop a model for a microchannel heat exchanger based on thermodynamic balances, heat transfer models, and semi-empirical correlations that tie a microchannel heat exchanger's geometry to its performance. Microchannel heat exchangers have been shown to provide significant increases in performance over conventional heat exchangers as seen in Section 2.4. Once this model is developed, it must be validated against published literature and then used to determine the optimal geometry and mass of the heat exchanger as a function of heat load.

The second objective is to use the heat exchanger models to parametrically compare microchannel heat exchangers to conventional plate fin heat exchangers using models initially developed by Gvozdich[4] and Weise[6] but modified and updated in this thesis research. This parametric comparison can then be used to draw conclusions about areas where the use of microchannel heat exchangers may be advantageous.

The third objective is to analyze the effect of fixed versus variable fin efficiency on the results for both the plate fin and microchannel heat exchanger models. Previous works by Gvozdich[4] and Weise[6] assumed a fixed fin efficiency in their plate fin heat exchanger model. By modifying the models to allow for a variable fin efficiency, the impact on both the performance and size of the exchangers can be analyzed.

The fourth and final objective is to analyze the effectiveness of different materials used in a phase change energy storage (PCES) system. These systems can provide additional performance boosts to an aircraft TMS as seen in Section 2.4. Using existing models developed by Gvozdich[4] a PCES system can be simulated to determine the impact of different materials on the performance of this system for the types heat loads generated by a solid- state DEWS. These heat loads are taken from those developed for a DEWS in Gvozdich[4].

Chapter 2 - Literature Review

This literature review highlights previous research on the design and modeling of TMS components for aerospace systems in the context of the optimization of aircraft in the conceptual design process.

2.1 Modeling and Analysis of Aircraft Thermal Subsystems

2.1.1 Aircraft Conceptual Design and Optimization

Aircraft conceptual design consists of creating a vehicle configuration to best meet the desired mission requirements and system specifications. In this phase of the design process, trade studies are conducted and the basic configuration of the aircraft is determined. The conceptual design phase lays the groundwork for all future phases in the design process.

The phase is also very important in terms of its impact on the final cost of the aircraft. As shown in Figure 2.1, dollars spent on trades, iterations, and design changes early in the design process (i.e., during the conceptual design phase) determines nearly 70% of the cost of a program[7].

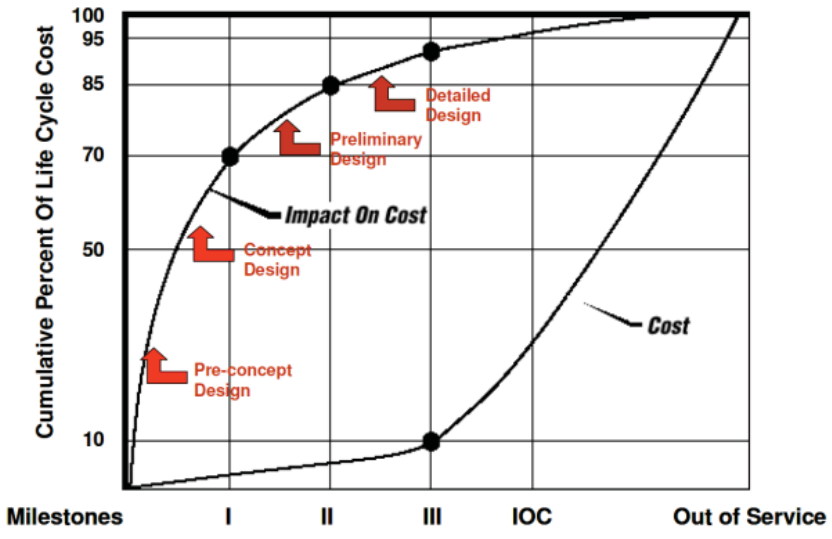

Figure 2.1 Cost of change in the design process. "Cost of Design Process Change". Defense Systems Management College. 2015.[b]

[b] Figure 2.1 is taken from material that is a work of the U.S. Government and not subject to copyright protection in the United States

In order to make better decisions earlier in the design process, there is increasing use of multidisciplinary design optimization (MDO) frameworks that attempt to integrate all required disciplines and facilitate complex multidisciplinary interactions in an effective manner[9]. MDO is enabled by modeling and simulation of the various aircraft subsystems and components. This allows for each of the subsystems to be coupled with each other and enables the flow of information between different disciplines[10]. For example, the model of the TMS requires an estimate of the heat loads from the power electronics subsystem. These subsystem models can be linked together so as to pass data back and forth among each other, allowing for each to run on data needed from the others.

MDO can be used to simultaneously optimize subsystems given a certain mission. This allows these subsystems to be designed to work with each other and helps to minimize conflicts between subsystems later in the design process. This allows for reductions in the cost of a program by preventing the need for redesigns late in the design process that drive the cost upwards.

Historically, thermal modeling has been relegated to the later phases of the design process for an aircraft, and as well detailed thermal management subsystem models have not been included in the conceptual design phase. However, as the electric power and thermal management requirements rapidly increase in aerospace systems, this approach is no longer valid[10]. Thermal management is becoming a limiting design factor for an aircraft's electrical subsystems and has become a factor that must be taken into account earlier in the design process[10, 11].

As seen above, the cost of potential changes to different subsystems is minimized the earlier they are evaluated in the design process. It has been seen that in order to mitigate configuration issues later in the design process, strategic design of the TMS must be incorporated earlier in the design process[12]. For example, assumptions and simplifications currently made about the TMS early in the design process may not hold for the final system design. This leads to costly redesigns later in the design process after the configuration of the other aircraft subsystems has already been finalized.

2.2 Tip-to-Tail Aircraft Modeling

Data from tip-to-tail modeling done by Weise[5] and Gvozdich[4] is used here to complete the present work. In their models, six different linked subsystems are modeled together. These subsystems are briefly described in the following sections.

2.2.1 Aircraft Vehicle Subsystem (AVS)

The aircraft vehicle subsystem (AVS) consists of the body of the aircraft. The AVS provides the lift and control surface movements that allow the aircraft to fly. The AVS also houses all of the other subsystems of the aircraft. Because of this, the AVS greatly affects the way the aircraft performs and has a large impact on the other subsystems.

The AVS model simulates the vehicle's motion using a 6 degree-of-freedom (DoF) model. For this model to work, the environmental conditions and vehicle weight from the fuel TMS (FTMS) are used as inputs. Using this data, the model can calculate the current vehicle range, endurance, and other parameters. The thrust requirements can then be sent to the engine controller, which varies the fuel rate to the engine[13].

2.2.2 Propulsion Subsystem (PS)

The propulsion subsystem (PS) is linked to the other subsystems through many dynamic interfaces. The AVS model calculates the thrust the engine (PS) needs to produce, and the PS returns the fuel flow rate needed so that the vehicle weight can be updated. The robust electrical power subsystem (REPS) then calculates a torque load that is applied to the engine shaft, and the PS takes this data and calculates the shaft speed necessary to produce this torque. The fuel flow rate needed is supplied from the FTMS to the PS, and the PS then recirculates any fuel used for cooling back to the FTMS. Bleed air from the engine is extracted from the engine by the adaptive power and TMS (APTMS) to power the integrated power pack (IPP) and cool different subsystem components. Finally, the high power electric actuation subsystem (HPEAS) calculates the forces on the control surfaces[13].

2.2.3 Electrical Subsystems

There are two primary electrical subsystems implemented in Weise's work[5]. These are the HPEAS and the REPS. For the work done in Gvozdich[4], the REPS and the HPEAS loads are

simplified to a duty cycled based lookup table and the 6-DOF model is replaced by a drag-polar model.

2.2.4 Thermal Management Subsystems

There are two primary thermal management subsystems: the FTMS and the APTMS. These subsystems contain heat exchangers that use fuel, RAM air, and closed-loop PAO subsystems to manage the heat loads from the other subsystems.

2.2.4.1 Fuel Thermal Management Subsystem (FTMS)

The FTMS model has several key responsibilities. They are as follows[4]:

1. The FTMS manages thermal loads from any DEWS onboard the aircraft. This is critical as the performance of a DEWS is directly liked to maintaining its laser diode arrays within a certain highly constrained temperature band.
2. The FTMS is responsible for keeping the temperature of the fuel below that of its vaporization temperature. Fuel is used as a heat sink for the aircraft and is used to help cool various other aircraft components. However, for survivability the fuel must be kept below its vaporization temperature to reduce the risk of explosion.
3. The FTMS contains the tip-to-tail's models of the fuel tank and pumps. It controls fuel flow rates to the PS[13].
4. The FTMS sends fuel to a vapor compression subsystem (VCS) in the APTMS. This VCS uses bleed air from the engine fan to cool the fuel before it is recirculated back into the fuel tanks.

2.2.4.2 Adaptive Power and TMS (APTMS)

The APTMS has several responsibilities for managing and powering several different subsystem components. These include the following[4]:

1. The APTMS contains the IPP, essentially a turbo-shaft engine that combusts fuel with bleed air to create power.
2. The APTMS includes heat exchangers that interact with closed PAO loops to keep the liquid-cooled avionics from overheating. The PAO temperature is maintained via an interaction with the fan bleed air through these heat exchangers.

3. The APTMS includes bleed air from the PS that is split into two streams used to cool the air cooled avionics and the cockpit. These streams are then rejected to the atmosphere.

An overall schematic of the tip-to-tail model is given in Figure 2.2.

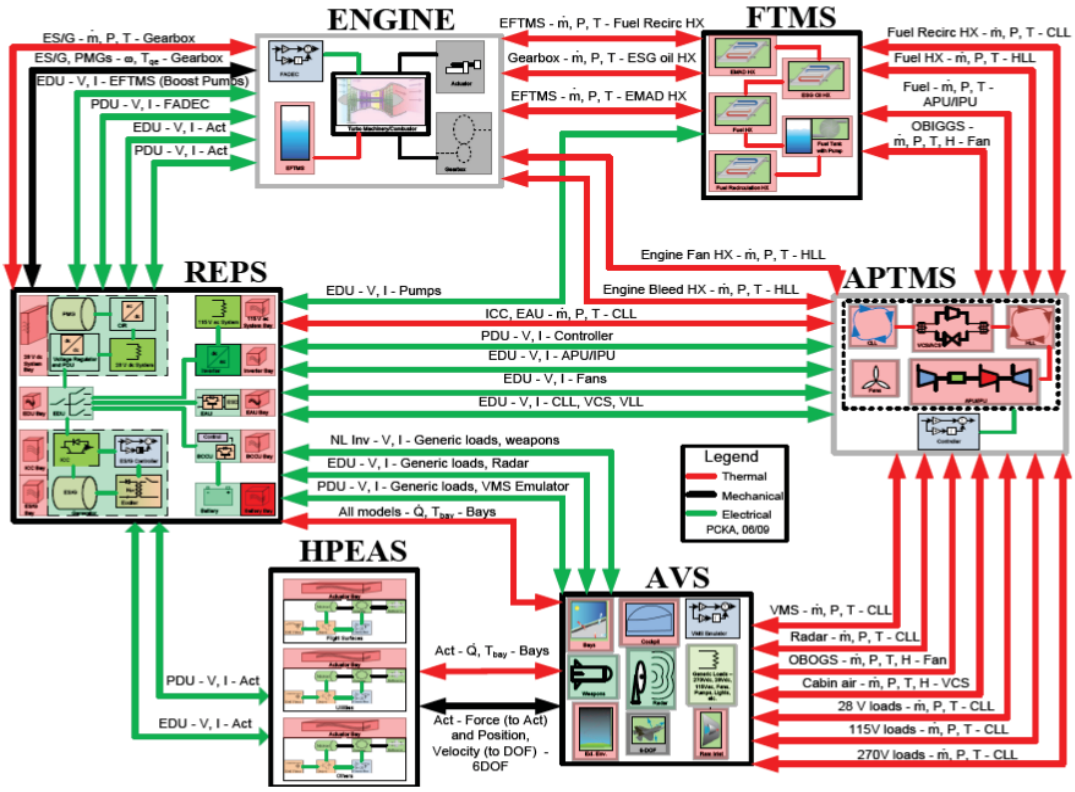

Figure 2.2 Essential aircraft sub-systems that form the tip-to-tail model. Gulczinski, F., "Integrated Vehicle Energy Technology Overview", D.o. Defense, Editor. 2012, Air Force Research Lab.[c]

2.3 Heat Exchanger Modeling and Simulation

There are many different forms of heat exchangers that exist for a variety of different applications. Some of the more common types of compact heat exchangers include[15]

- plate-fin heat exchangers
- tube-fin heat exchangers
- diffusion-bonded heat exchangers
- plate-frame heat exchangers

[c] Figure 2.2 is taken from material that is a work of the U.S. Government and not subject to copyright protection in the United States

- plate-shell heat exchangers

2.3.1 Plate-Fin Heat Exchanger

The plate-fin heat exchanger is one of the more common heat exchanger types in use today. Plate-fin heat exchangers benefit from relatively high performance and a low production cost. These heat exchangers vary in both their fin structure and the way their layers are stacked. Some of the more common fin configurations are depicted in Figure 2.3 from Hesselgreaves[15].

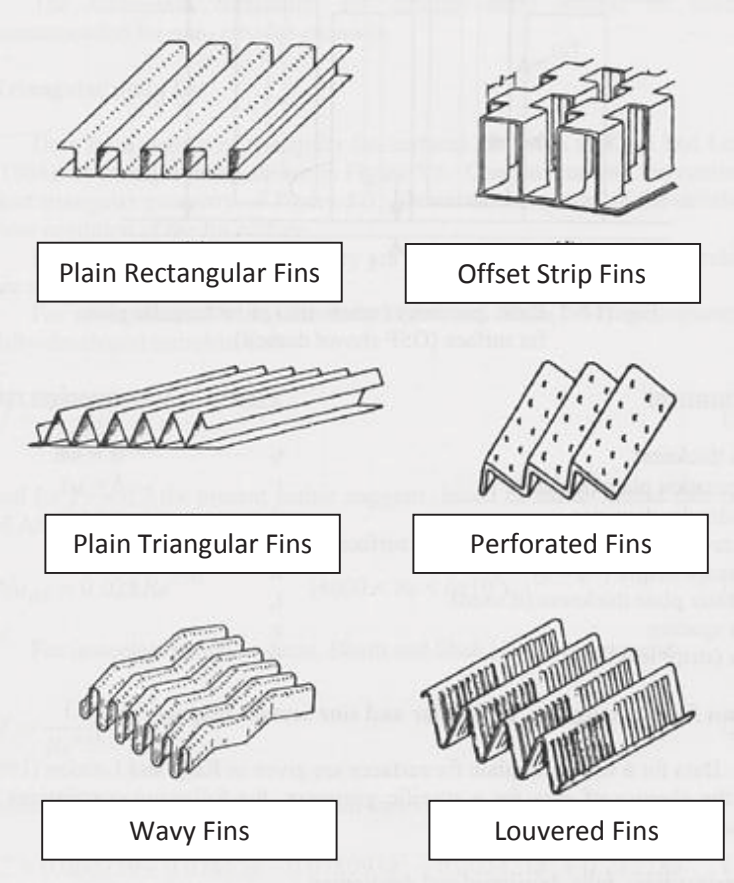

Figure 2.3 Plate fin heat exchanger fin geometries. Hesselgreaves, J.E., *Compact heat exchangers: selection, design and operation*. 2001: Gulf Professional Publishing. Used under fair use, 2015

Plate-fin heat exchangers are also characterized by the relative flow direction of both the hot and cold streams. These include parallel flow where both flows move through the exchanger in the same direction, cross flow where the flows move at right angles to each other, and counter

flow where the flows move in opposing directions through the exchanger. An example of both a tube-fin and plate-fin heat exchanger is given in Figure 2.4.

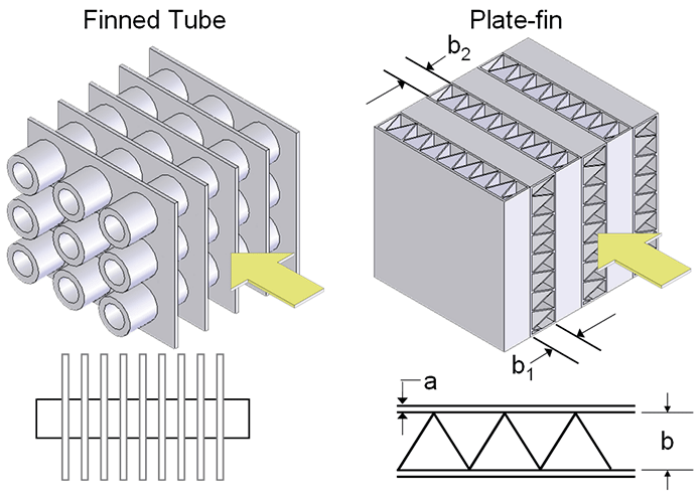

Figure 2.4 Tube-fin versus Plate-fin heat exchanger. "Finned Tube versus Plate Fin Heat Exchanger". 2015. http://fchart.com/ees/heat_transfer_library/compact_hx/hs100.htm. Used under fair use, 2015

2.3.2 Heat Exchanger Sizing, Modeling, and Simulation in the Literature

In order to develop accurate heat exchanger models, it is necessary to validate a model not only by actual numbers but by its general behavior. In order to do this, several different sources such as Kays and London[17], Shah[18], and Hesselgreaves[15] are consulted to develop a heat exchanger sizing algorithm.

In order to size the heat exchangers, a general sizing technique taken from Hesselgeaves is used. This technique is valid for counter flow heat exchangers and is divided into two stages as follows.[5, 15]

Stage 1 Scoping size

- For a given thermal specification, calculate the heat exchanger effectiveness.
- For given heat capacity rates for both the hot- and cold- side fluids calculate the ratio of heat capacity rates.
- Estimate the overall NTU (number of transfer units)
- Calculate the NTU for each side.
- Calculate the mass velocity for each side based on an initial estimate of the NTU for each side and an initial guess for the pressure drop.

- Based on the fin characteristics and design flow rates, calculate the Reynolds number for each side.
- Calculate the overall heat exchanger length for each side.

Stage 2 Counter-flow design

- Calculate the geometric mean of the lengths calculated in the previous stage.
- Calculate a new pressure drop.
- Calculate a new effectiveness and overall NTU.
- Compare the calculated effectiveness with the desired effectiveness.
- Calculate a new overall heat exchanger length and iterate until the effectiveness converges.

The sizing process for plate-fin heat exchangers used later in this work is derived from this process and outlined further in *Chapter* 3.

2.4 Advanced Heat Exchanger and Thermal Management Technology

2.4.1 Microchannel Heat Exchangers

There is a great deal of research being done on improving heat exchanger technology. Several different technologies are being studied to develop heat exchangers that can outperform current technology while reducing the weight and volume needed to complete the mission. One of the technologies being investigated is the use of microchannel heat exchangers.

Heat exchangers with hydraulic diameters less than 1 mm are generally considered to be microchannel heat exchangers[19]. These heat exchangers are good for high heat flux removal applications such as those in an aircraft TMS as they have good thermal performance with an extremely compact size. Traditionally, these types of heat exchangers have been used for the thermal management of microelectronic devices. However, research is being conducted to determine their use in other applications[20].

Microchannel heat exchangers are able to achieve greater heat transfer performance via a significant increase in the heat transfer surface area. These exchangers are characterized by a small fin-spacing-to-height aspect ratios as well as small hydraulic diameters of the flow passages that are generally less than 1 mm[20]. These features allow for higher heat transfer

coefficients than those of comparable plate-fin heat exchangers. Because of this, previous work has seen 20% to 30% reductions in mass between plate fin heat exchangers and microchannel heat exchangers. This is demonstrated in Figure 2.5 from the work done by Honeywell where an offset plate-fin design is compared with microchannel heat exchangers that are originally constrained to the same envelope as the plate-fin heat exchanger and then allowed to exceed this envelope[20].

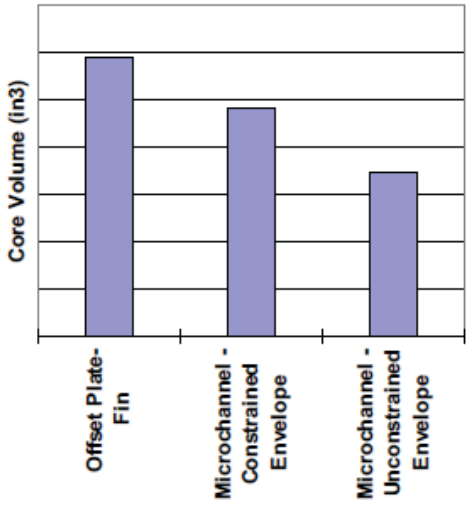

Figure 2.5 Comparison of plate fin versus microchannel core volumes. Williams, M., et al., "Advanced heat exchanger technology for aerospace applications". 2008, SAE Technical Paper. p64. Used under fair use, 2015

2.4.1.1 Manufacturing Challenges of Microchannel Heat Exchangers

Microchannel heat exchangers while promising have their own manufacturing challenges that can limit their performance. For these heat exchangers, the interior geometry of the exchanger is driven by the workability of the desired material and the manufacturing processes that can be used on that material[20]. These factors can limit variables such as fin height, fin thickness, and fin spacing, thus limiting the available performance of these heat exchangers.

In order to overcome these manufacturing challenges, various new methods of manufacturing microchannel heat exchangers are being developed. Some of these methods include micro-machining, stereolithography, and chemical etching[21]. Micro-machining typically involves either diffusion bonding where two surfaces are bonded together under high temperatures and mechanical pressure or the use of diamond tools to mill or grid the material into shape.

Stereolithography is a process by which a UV light ray scans through a reactive liquid polymer. This causes a reaction that hardens the polymer, creating a thin solid layer. This solid layer is then lowered slightly and the process is repeated, building layer upon layer on top of each other. This polymer structure can then be formed into a ceramic by a heat cuing process known as pyrolysis.

2.4.2 Phase Change Energy Storage

Phase change energy storage (PCES) is another method being actively researched to increase the performance of aircraft TMS. Gvozdich[4] and Shanmugasundaram[22] have evaluated the potential benefits of using PCES as a thermal management option for pulsed power and DEWSs. The benefit of PCES is that this method uses latent energy storage. Latent energy storage utilizes the fact that during a phase change the temperature of the PCM does not change. The PCM absorbs energy and this energy enacts the phase change without raising the temperature. This is in contrast to sensible heat storage, which uses a change in temperature in the storage medium as the energy storage method. Because of this, sensible heat storage devices must be sized much larger in order to store an equivalent amount of energy as latent heat storage devices without having large swings in temperature or temperatures that exceed the operating limitations of the overall TMS.

In Shanmugasundaram[22], a composite substance of wax and carbon fiber is used as a phase change material (PCM). Paraffin wax is infused into a structure of K1100 carbon foam with a porosity of 0.8. The reason for using the carbon foam is that paraffin wax on its own does not have a high thermal conductivity. This could lead to sharp temperature gradients in the phase change material, decreasing performance. The physical and thermal properties of the paraffin wax and K1100 carbon foam are given in Table 2.1.

The thermal energy storage (TES) cell used is sized using knowledge of a DEWS duty cycle, heat load, and the heat of fusion for the paraffin wax. The PCM is enclosed in a hermetic shell with the working fluid passing over its surface. This model assumes a near-infinite effective thermal conductivity and negligible sensible heat. A schematic of the TES cell used by Shanmugasundaram is shown in Figure 2.6.

Table 2.1 List of TES parameters Shanmugasundaram, V., et al. "Aircraft Based Pulsed Power System Thermal Management Options With Energy Storage". in *4th International Energy Conversion Engineering Conference, San Diego, California*. 2006. Used under fair use, 2015

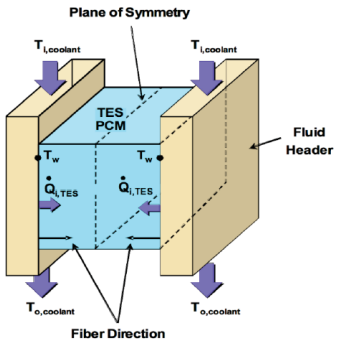

Tube on	t_{on}	15	s
Heat load	Q	2845	kW
ΔT across heat load	$(\Delta T)_{load}$	69.6	°C
PCM melt temperature	$T_{PCM,melt}$	327.5	K
PCM heat of fusion	$h_{PCM,SL}$	200	kJ/kg
PCM density	ε_{PCM}	850	kg/m^3
PCM thermal conductivity	κ_{PCM}	0.2	W/m-K
Porosity	ε	0.8	
K1100 thermal conductivity	κ_{K1100}	1100	W/m-K
K1100 density	ε_{K1100}	2200	kg/m^3
PCM effecive density	ε_{eff}	1120	kg/m^3
PCM effecive thermal conductivity	κ_{eff}	220.16	W/m-K

Figure 2.6 TES cell schematic. Shanmugasundaram, V., et al. "Aircraft Based Pulsed Power System Thermal Management Options With Energy Storage". in *4th International Energy Conversion Engineering Conference, San Diego, California*. 2006. Used under fair use, 2015

Work done by Gvozdich[4] on modeling a TES cell analyzes the effect of discretizing the TES cell into a 2D model and analyzing the effect this had on the results. For these tests, a quasi-2D model as well as a full 2D model are created. Both of these models are discretized in the axial flow direction with convective heat transfer occurring in the direction perpendicular to the flow path. The quasi-2D model assumes lumped capacitance in the direction perpendicular to the flow path while the 2D model is discretized in this direction. The discretization schemes for the quasi-2D and 2D models are shown in Figures 2.7 and 2.8, respectively.

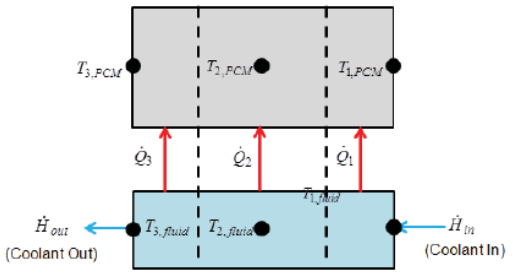

Figure 2.7 Example of the discretization scheme for the quasi-2D TES PCM model. Gvozdich, G., "Modeling the Effects of Transient High Energy Weapon Subsystems on High-performance Aerospace Systems, in Mechanical Engineering". 2011, M.S. thesis advisor: M.R. von Spakovsky, ME dept., Virginia Tech Blacksburg, VA. Used with Permission of Grant Gvozdich, 2015

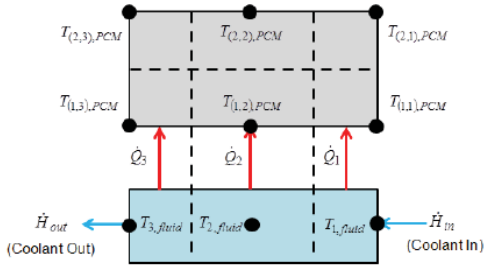

Figure 2.8 Example of the discretization scheme for the 2D TES PCM model. Gvozdich, G., "Modeling the Effects of Transient High Energy Weapon Subsystems on High-performance Aerospace Systems, in Mechanical Engineering". 2011, M.S. thesis advisor: M.R. von Spakovsky, ME dept., Virginia Tech Blacksburg, VA. Used with Permission of Grant Gvozdich, 2015

For a TES cell designed for a 10 second lasing of a 100 kW DEWS, 23.9 kilograms of PCM was needed. Using a constant inlet temperature of 300 K, water is used as the working fluid and the PCM is started at a temperature of 280 K. The time for the cell to reach a uniform temperature of 300 K is used as the charge time.

As can be seen in Table 2.2, there are significant differences between the qusi-2D and 2D PCM models. It is seen that using the lumped capacitance assumption in the quasi-2D model causes the charge time of the PCS cell to be significantly lower than that of the discretized 2D cell. This led Gvozdich[4] to conclude that discretizing the TES cell in two dimensions is important to the final results and that the lumped-capacitance model is insufficient for these types of models. Also, due to the increasing simulation time due to the addition of more nodes perpendicular to the flow path, the optimal 2D discretization scheme for the TES model includes around 5 nodes in the perpendicular direction.

Table 2.2 Results for the 2D and quasi-2D TES PCM models for a simulation time of 200 sec. Gvozdich, G., "Modeling the Effects of Transient High Energy Weapon Subsystems on High-performance Aerospace Systems, in Mechanical Engineering". 2011, M.S. thesis advisor: M.R. von Spakovsky, ME dept., Virginia Tech Blacksburg, VA. Used with Permission of Grant Gvozdich, 2015

Number of Nodes in the Direction Perpendicular to the Coolant Flow	**Charge Time**	**Run Time**
-	[s]	[s]
1	8	0.59
2	157	0.69
5	146	0.79
10	146	1.37
20	142	4.65

Chapter 3 - Model Formulation

For this M.S. thesis research models are developed to size both a microchannel heat exchanger as well as a PCES cell for various loading conditions. Details of the microchannel model are given in *Sections* 3.1 and 3.2 and of the phase change model in *Section* 3.3.

3.1 Development of the Microchannel Heat Exchanger Sizing Algorithm

The equations and parameters governing the physical dimensions of a microchannel heat exchanger are given in Table 3.1. For this research, an offset-strip-fin microchannel heat exchanger is modeled as this type of exchanger typically delivers a higher performance-to-weight ratio then other types of heat exchangers[15]. The physical geometry of this type of exchanger is shown in Figure 3.1.

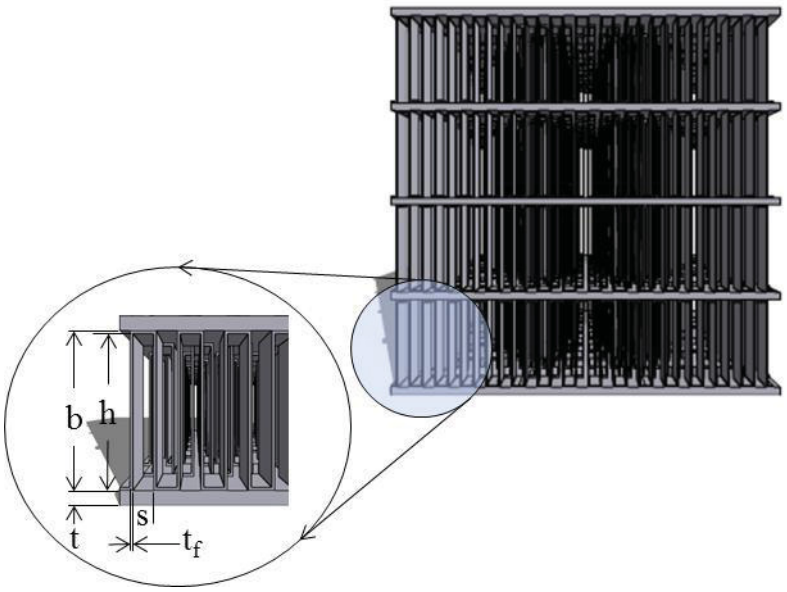

Figure 3.1 Schematic of a typical counter-flow microchannel heat exchanger. Weise, P., "Mission-Integrated Synthesis/Design Optimization of Aerospace Systems under Transient Conditions", in *Mechanical Engineering*. 2012, M.S. thesis advisor: M.R. von Spakovsky, ME dept., Virginia Tech: Blacksburg, VA. Used with permission of Peter Weise, 2015.

For a microchannel heat exchanger model, there are five key geometric characteristics, namely, these are the hydraulic diameter D_h; the porosity, σ; and the non-dimensional aspect ratios α, δ, and γ defined in Table 3.1. The hydraulic diameter is used as the characteristic length in the Reynolds number equation. Because Reynolds number is directly used in the heat transfer equations, the hydraulic diameter is a key component of the microchannel model. With a lower

hydraulic diameter, the Reynolds number is lowered, while the convective heat transfer coefficient is raised. Because of this, low hydraulic diameters such as those used in microchannel heat exchangers are desirable for higher heat exchanger performance with lower weight. Porosity is also important as it is a measure of heat exchanger compactness. It is defined as the ratio of the wetted volume to the total volume of the heat exchanger. In addition, the non-dimensional aspect ratios are significant since they are used in the correlations to determine *f,* the Fanning friction factor, and *j*, the Colburn coefficient. This factor and coefficient have a direct impact on both the pressure drop and mass velocity through the exchanger, making them key variables in the design model. Table 3.1 details the relationships between these key parameters and the microchannel heat exchanger dimensions.

Table 3.1 Geometry equations for a microchannel heat exchanger.

Variable	Description	Model Equation
D_h	Hydraulic Diameter (m)	$D_h = \frac{2sh}{(s+l)}$
σ	Porosity (m^3/m^3)	$\sigma = \frac{s(b-t_f)}{(s+t_f)(b+t)}$
β	Surface area density of one side of heat exchanger (m^2/m^3)	$\beta = \frac{4\sigma}{D_h}$
s	Fin channel width (m)	$\alpha = \frac{s}{h}, \delta = \frac{t_f}{l}, \gamma = \frac{t_f}{s}$
h	Fin Channel Height (m)	
l	Fin Strip Length (m)	
b	Plate Gap Thickness (m)	
t_f	Fin Thickness (m)	
t	Plate Thickness (m)	
L	Overall Heat Exchanger Length (m)	
α	Non-dimensional aspect ratio	
δ	Non-dimensional aspect ratio	
γ	Non-dimensional aspect ratio	

As described in Hesselgreaves[15] and Weise[6], an iterative process is used to size the microchannel heat exchanger's flow area. This process is similar to that used to size a conventional compact offset-strip-fin heat exchanger. An iterative process is needed to size the

heat exchanger area due to the fact that in order to calculate the Reynolds number of the flow, there must be knowledge of the fluid flow velocity in the heat exchanger. This velocity is a function of both the volumetric flow rate and flow areas of which only the volumetric flow rate is known. In order to find the flow area, an initial estimate must be made, termed $A_{c,0}$. By working through the equations, a mass velocity, *G*, can be determined. This mass velocity is a function of both the mass flow rate and the flow area. The flow area can then be determined. However, if the initial estimate of the flow area is incorrect, this calculated flow area is also incorrect. Thus, an iterative process is required where the result from the previous iteration for the flow area is used as the initial guess for the flow area in the next iteration until convergence is reached. With a sufficiently close initial guess, there is typically a fast convergence using this process. A more detailed description of the iterative process is given as follows[6]:

1. Select the physical parameters of the heat exchanger such as *b, h, t, s, t_f, L.*
2. Calculate the hydraulic diameter, D_h.
3. Provide an estimate of the heat exchanger flow area and calculate the Reynolds number.
4. Use the Reynolds number and the non-dimensional aspect ratios from Table 3.1 to calculate the Colburn coefficient, *j*, and the friction factor, *f*. The correlations used to calculate these, given in Table 3.2, have been demonstrated in Hesselgreaves[15] to be valid for both the laminar and turbulent flow regimes.
5. Determine the heat exchanger effectiveness using the effectiveness-NTU method
6. Calculate the pressure drop and mass velocity.
7. From the mass velocity, calculate a new flow area. If this new flow area differs from the previous guess by more than a given tolerance, iterate until this tolerance is met.
8. Once the flow area converges, calculate the weight, volume, and surface area of the heat exchanger.

A flowchart of this iterative process is given in Figure 3.2[5]. Figure 3.3 gives a schematic of the heat exchanger thermodynamic system[4]. The equations used are given in Tables 3.2[6,15], 3.3, and 3.4.

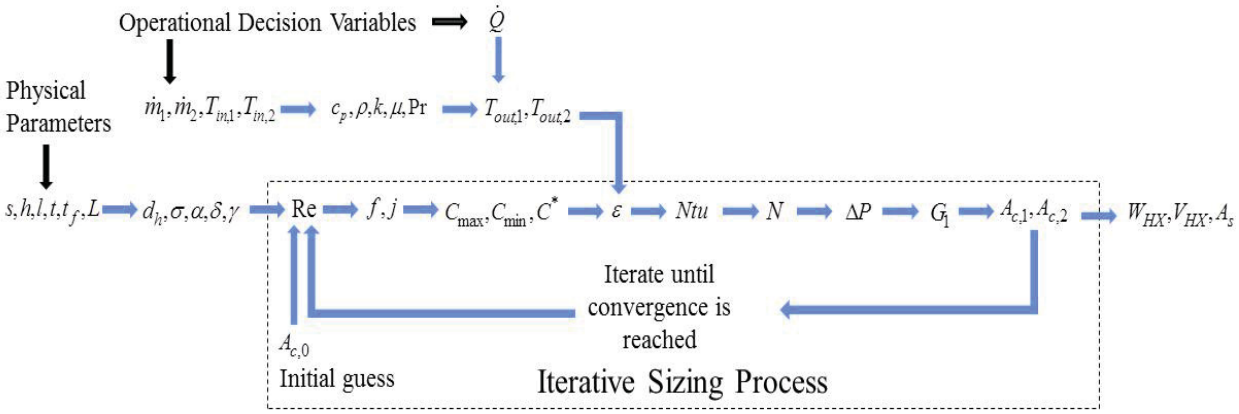

Figure 3.2 Iterative sizing process for area. Weise, P., "Mission-Integrated Synthesis/Design Optimization of Aerospace Systems under Transient Conditions", in *Mechanical Engineering*. 2012, M.S. thesis advisor: M.R. von Spakovsky, ME dept., Virginia Tech: Blacksburg, VA. Used with permission of Peter Weise, 2015.

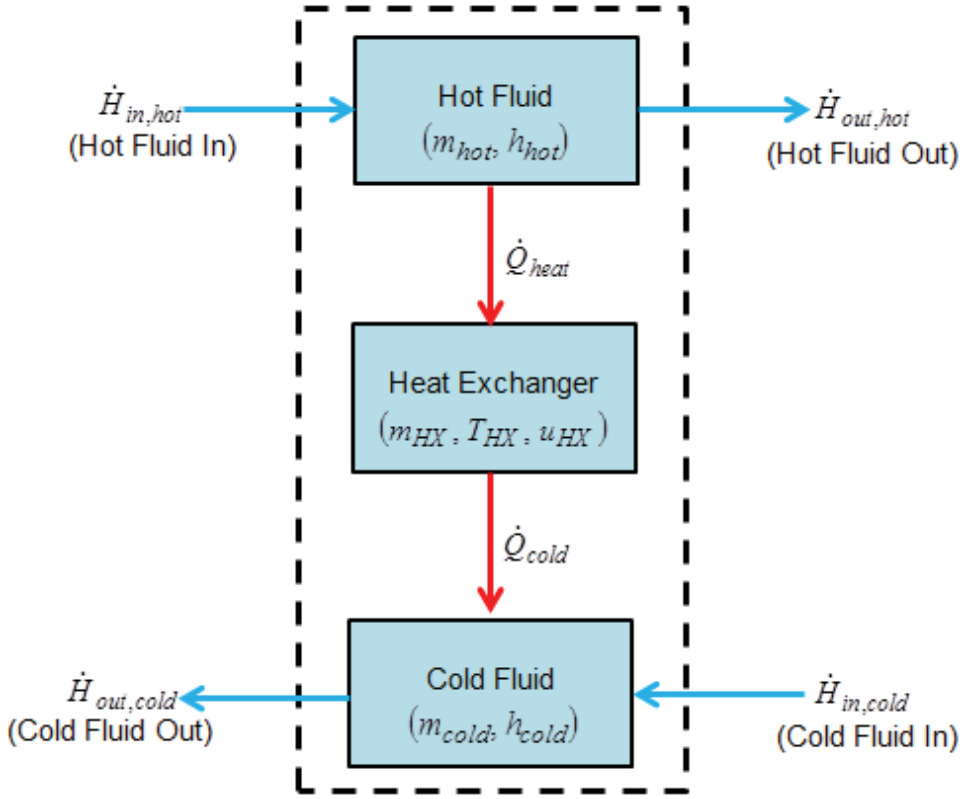

Figure 3.3 Heat exchanger thermodynamic system. Gvozdich, G., "Modeling the Effects of Transient High Energy Weapon Subsystems on High-performance Aerospace Systems, in Mechanical Engineering". 2011, M.S. thesis advisor: M.R. von Spakovsky, ME dept., Virginia Tech Blacksburg, VA. Used with Permission of Grant Gvozdich, 2015

Table 3.2 Iterative design heat transfer and pressure drop equations

Variable	Description	Model Equation
f	Fanning Friction Factor	$f = 9.6243Re^{-0.7422}\alpha^{-0.1856}\delta^{0.3053}\gamma^{-0.2659} * (1 + 7.669 * 10^{-8}Re^{4.429}\alpha^{0.92}\delta^{3.767}\gamma^{0.236})^{0.1}$
j	Colburn coefficient	$j = 0.6522Re^{-0.5403}\alpha^{-0.1541}\delta^{-0.1409}\gamma^{-0.0678} * (1 + 5.269 * 10^{-5}Re^{1.34}\alpha^{0.504}\delta^{0.456}\gamma^{-1.055})^{0.1}$
ε	Heat Exchanger Effectiveness	$\varepsilon = \frac{Q}{Q_{Max}} = \frac{\dot{Q}}{(\dot{m} * c_p)_{min}(T_{1,i} - T_{2,i})}$
$\dot{Q}$	Heat Load (W)	
$\dot{Q}_{max}$	Design Heat Load (W)	
NTU	Number of Thermal Units	$NTU = \frac{\varepsilon}{1-\varepsilon}$ $\quad N = \frac{2NTU}{\eta_0}$
N	NTU for one side	
$A_{c,fluid}$	Fluid Flow Area (m^2)	$\Delta p = \frac{1}{2}\rho f\left(\frac{\dot{m}}{A_c}\right)^2\left(\frac{4L}{D_h}\right)$ $\quad G_1 = \frac{\dot{m}_1}{A_{c,1}} = \sqrt{\frac{2\rho_1\Delta p_1\frac{j_1}{f_1}}{Pr_1^{\frac{2}{3}}N}}$
Δp	Pressure Drop (Pa)	
G	Mass Velocity (kg/m^2s)	$Re = \frac{\rho u D_h}{\nu}$

Table 3.3 Effectiveness-NTU equations

Variable	Description	Model Equation
C_{min}	Minimum Heat Capacity (J/K)	$C_{min} = \min(C_{hot,in}, C_{cold,in})$
C_{max}	Maximum Heat Capacity (J/K)	$C_{max} = \max(C_{hot,in}, C_{cold,in})$
$\dot{Q}_{max}$	Maximum Heat Transfer (W)	$\dot{Q}_{max} = C_{min}(T_{hot,in} - T_{cold,in})$
		$\dot{Q}_{heat} = \varepsilon * \dot{Q}_{max}$
ε	Effectiveness	$C^* = \frac{C_{min}}{C_{max}}$
C^*	Heat Capacity Ratio	$\varepsilon = \frac{1 - e^{-NTU(1-C^*)}}{1 - C^* * e^{-NTU(1-C^*)}}$
NTU	Number of Thermal Units	$NTU = \frac{\varepsilon}{1-\varepsilon}$

Table 3.4 Heat exchanger mass, volume, and area equations

Variable	Description	Model Equation
m_{hx}	Mass of heat exchanger (kg)	$m_{hx} = \rho_m L\left(\frac{A_{c,1}}{\sigma_1}(1-\sigma_1)+\frac{A_{c2}}{\sigma_2}(1-\sigma_2)\right) + (A_{c1}\rho_1 + A_{c2} + \rho_2)L$
V_{hx}	Volume of heat exchanger (m^3)	$V_{hx} = L\left(\frac{A_{c,1}}{\sigma_1}(1-\sigma_1)+\frac{A_{c2}}{\sigma_2}(1-\sigma_2)\right)$
A_s	Surface area of one side of heat exchanger (m^3)	$A_s = \beta\left(\mathrm{L}\left(\frac{A_c}{\sigma}(1-\sigma)\right)+A_c\right)$

The first step in the iterative process seen in Figure 3.2 is to use the desired heat transfer rate to determine the fluid outlet temperatures out of the heat exchanger. Using this, geometry parameters described in Table 3.1, and an estimate of the fluid flow area the Reynolds number and the flow properties can be determined using the equations given in Table 3.2. Then, using the equations given in Tables 3.2 and 3.3 the heat transfer properties such as the number of transfer units and effectiveness of the heat exchanger can be determined. Using these heat transfer properties the pressure drop and mass velocity through the exchanger can be determined. From this mass velocity, a new estimate for the fluid flow area can be determined from equations in Table 3.2. This new estimate can then be used as an initial guess for the next iteration. Once convergence is met, the mass and volume of the heat exchanger can be determined using equations given in Table 3.4.

For the above process to be valid, there are several assumptions that must be made. These assumptions include incompressible flow within the heat exchanger and constant properties such as specific heat, density, and viscosity. Another assumption made in previous work is that the fin efficiency be fixed at 0.7[6, 15]. This assumption had been proven to be realistic for moderate heat transfer coefficients and commonly used materials. It is being used for the first part of the modeling done in this thesis. However analysis of how allowing a variable fin efficiency affects the results is also conducted. This analysis is done using the equations in Table 3.5[24]:

Table 3.5 Variable fin-efficiency equations

Variable	Description	Model Equation
η	Fin Efficiency	$\eta = \frac{Q_{act}}{Q_{max}} = \frac{\tanh(mL)}{mL}$ $m = \left(\frac{2h}{kt_f}\left(1 + \frac{t_f}{l}\right)\right)^{\frac{1}{2}}$ $L = \frac{L_{fin}}{2} - t_f$
h	Convective Heat Transfer Coefficient $(\frac{W}{m^2K})$	
A_{fin}	Fin Surface Area (m^2)	
k	Thermal Conductivity of Fin $(\frac{W}{mK})$	
$A_{c,fin}$	Fin Cross Sectional Area (m^2)	
L_{fin}	Fin Length (m)	
t_f	Fin Thickness (m)	

Table 3.6 describes the equations used to determine the convective heat transfer coefficients of the microchannel heat exchanger. Based on the Reynolds number and Prandtl number of the fluid, the appropriate correlation for the Nussult number is determined from Table 3.7[6,25]. This number is then used to get the convective heat transfer coefficient of the fluid which is used in Table 3.5 in the determination of the fin efficiency.

Table 3.6 Equations to determine the wall heat transfer coefficient.

Variable	Description	Model Equation
h	Convective Heat Transfer Coefficient $\left(\frac{W}{m^2K}\right)$	$h = \frac{Nuk_f}{D_h}$ $Nu = g(f, Re, Pr, D_h)$ $Pr = \frac{C_p\mu}{k_f}$
Nu	Nussult Number	
k_f	Fluid Thermal Conductivity $\left(\frac{W}{mK}\right)$	
D_h	Hydraulic Diameter (m)	
f	Friction Factor	
Re	Reynolds number	
Pr	Prandtl Number	

Table 3.7 Gnielinski correlations for determining turbulent flow Nussult number.

Model Equation	Valid Range	
	Reynold's Number	**Prandtl Number**
$Nu = \frac{\left(\frac{f}{2}\right)(Re-1000)Pr}{1+12.7(\frac{f}{2})(Pr^{\frac{2}{3}}-1)}\left[1+\left(\frac{D_h}{L}\right)^{\frac{2}{3}}\right]$	$2300<Re<5\text{x}10^4$	$0.2<Pr<2000]$
$Nu = 0.0214(Re^{0.8}-100)Pr^{0.4}\left[1+\left(\frac{D_h}{L}\right)^{\frac{2}{3}}\right]$	$10^4<Re<5\text{x}10^5$	$0.5<Pr<1.5$
$Nu = 0.012(Re^{0.87}-280)Pr^{0.4}\left[1+\left(\frac{D_h}{L}\right)^{\frac{2}{3}}\right]$	$3\text{x}10^3<Re<10^6$	$1.5<Pr<500$
$Nu = 0.023\left(Re^{4/5}-280\right)Pr^{0.3}$	$Re > 10^6$	$0.6<Pr<160$

3.2 Microchannel Heat Exchanger Sizing Optimization

The weight and size of microchannel heat exchangers depend on both the operational decision variables (flow rate, temperature, and pressure) and the fin geometry. Fin geometry is one of the key factors affecting heat exchanger mass and volume. Because of this, an optimization routine is run to determine the fin geometry that gives the lowest heat exchanger mass, while meeting certain constraints. This optimization problem can be defined as follows:

Minimize:

$$m_{hx} = \rho_m L\left(\frac{A_{c,1}}{\sigma_1}(1-\sigma_1)+\frac{A_{c2}}{\sigma_2}(1-\sigma_2)\right)+(A_{c1}\rho_1+A_{c2}+\rho_2)L \tag{3.1}$$

With respect to:

$$[s,\ h,\ l,\ t_f,\ t,\ L] \tag{3.2}$$

Subject To:

$$lb \leq \left[s,\ h,\ l,\ t_f,\ t,\ L\right] \leq ub \tag{3.3}$$

$$\Delta p \leq 30\ kPa \tag{3.4}$$

Where lb is the lower bound of the fin geometry parameters, ub is the upper bound on the fin geometry parameters, and Δp is the pressure drop across the heat exchanger. The constraint of $\Delta p \leq 30\ kPa$ is due to the limits of the pumping capacity in the Tip-to-Tail model used.

The lower and upper bounds for the fin geometry parameters are taken from Jiang[26], Mathew[19], and Shah[18]. They are shown in Table 3.8. The optimization algorithm used for this work is MATLAB's "fmincon" function. This function solves a constrained minimization problem of the form

$$\text{Min } f(x) \text{ such that } \begin{cases} c(x) \leq 0 \\ ceq(x) = 0 \\ A \cdot x \leq b \\ Aeq \cdot x \leq beq \\ lb \leq x \leq ub \end{cases} \tag{3.5}$$

where $x, b, beq, lb,$ and ub are vectors, A and Aeq are matrices, $c(x)$ and $ceq(x)$ are functions that return vectors, and $f(x)$ is a function that returns a scalar. For this study the objective function, $f(x)$, is the mass of the heat exchanger. Information on the "fmincon" function can be found via Mathwork's website. For the problem posed in equations (3.1) to (3.4), there are no linear constraints, leaving $A, Aeq, b,$ and beq unused. The nonlinear constraint used to generate $c(x)$ is that for the pressure drop, which cannot exceed 30 kPa.

Table 3.8 Upper and lower bounds for microchannel and plate-fin optimization decision variables.

		s_1	h_1	l_1	t_{f1}	t_1	s_2	h_2	l_2	t_{f2}	t_2	L
		mm	mm	mm	mm	mm	mm	mm	mm	mm	mm	m
Micro	Lower Bound	0.2	0.15	0.1	0.15	0.5	0.2	0.15	0.1	0.15	0.5	0.1
	Upper Bound	2.08	20	6.35	0.5	19	2.08	20	6.35	0.5	19	2.5
Plate Fin	Lower Bound	0.83	1.29	2.4	0.15	0.9	0.83	1.29	2.4	0.15	0.9	0.1
	Upper Bound	2.08	20	6.35	0.5	19	2.08	20	6.35	0.5	19	2.5

3.3 Thermal Energy Storage (TES) Model

In Gvozdich[4], thermodynamic and heat transfer models were developed for a TES cell. These models are used in this work to analyze how different materials affect the performance of a TES cell. The thermodynamic system used is illustrated in Figure 3.4. It consists of the TES cell and a working fluid. The equations governing this system are given in Table 3.9[4]. The TES cell is discretized into a 2D grid using a third order finite difference approach.

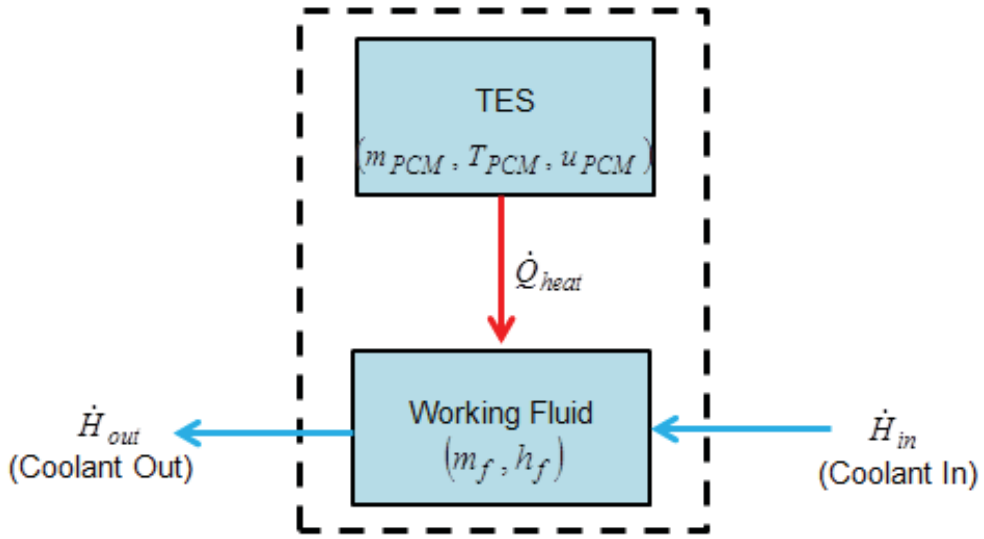

Figure 3.4 TES Thermodynamic System. Gvozdich, G., "Modeling the Effects of Transient High Energy Weapon Subsystems on High-performance Aerospace Systems, in Mechanical Engineering". 2011, M.S. thesis advisor: M.R. von Spakovsky, ME dept., Virginia Tech Blacksburg, VA. Used with Permission of Grant Gvozdich, 2015

Table 3.9 TES cell and working fluid thermodynamic equations.

Variable	Description	Model equation
u_{PCM}	PCM specific internal energy	$u_{PCM}(T_{PCM,2}) = u_{PCM,1} + \frac{1}{m_{PCM}} \int_{t_1}^{t_2} (\dot{Q_{heat}}) dt$ $h_f(T_{f,2}) = h_{f,1} + \frac{1}{m_f} \int_{t_1}^{t_2} (-\dot{Q}_{heat} + (\dot{m}h)_{f,in} - (\dot{m}h)_{f,out}) dt$
T_{PCM}	PCM temperature	
m_{PCM}	PCM mass	
$\dot{Q_{heat}}$	Heat transfer rate	
$(\dot{m}h)_{f,in}$	Fluid enthalpy flow rate into the system	
$(\dot{m}h)_{f,out}$	Fluid enthalpy flow rate out of the system	

In this system, fluid passes through channels attached to the surface of the TES cell. Depending on the gradient in temperature between the working fluid and the TES cell, the fluid exchanges energy with the PCM. The model assumes ideal, incompressible behavior in the working fluid.

The heat transfer between the PCM and the working fluid relies on two heat transfer mechanisms, conduction and convection. Energy enters or exits the TES cell through the surface in contact with the working fluid. Energy passes to this surface through convection in the working fluid and this energy is then diffused to the PCM throughout the TES cell via conduction. The interface between the TES and the working fluid is similar to that of a compact plate-fin heat exchanger. This allows the Gnielinski equations given in Table 3.7 to be used to determine the Nussult number and, thus, the convective heat transfer coefficient. The governing equations for this convective heat transfer are given in Table 3.10.

Table 3.10 Heat transfer model equation for TES cell

Variable	Description	Model equation
$\dot{Q_{heat}}$	Heat interaction with working fluid	$\dot{Q_{heat}} = hA_s(T_{fluid} - T_{surface,PCM})$
h	Film coefficient	
A_s	Effective heat transfer area	

In order to size the TES PCM cell, an operational heat load that needs to be stored is first determined. To absorb this heat load, the PCM must have a change in internal energy equal to it. Using this knowledge along with equations from Table 3.8, the mass needed to be able to hold this energy can be obtained.

Chapter 4 - Results

4.1 Microchannel Heat Exchanger Model Validation

In order to validate that the model created for the microchannel heat exchanger, data generated from the model was compared to that from the literature. Due to the fact that data with regard to the performance of offset-strip-fin compact heat exchangers as well as microchannel heat exchangers has limited availability, this validation is conducted with both previous sizing data as well as model trends.

The first evaluation that is done is to determine if the heat exchanger mass predicted by the model closely match that seen in previous work. In order to do this, two different test cases are run. These two test cases are for a heat exchanger under two different load conditions. These conditions are representative of the loads seen in the tip-to-tail model used by Gvozdich[4] and Weise[6]. In both test cases, a compact plate fin heat exchanger is sized using the model developed here. The environmental conditions used for these two tests are given in Tables 4.1 and 4.2 while geometries used for these two heat exchangers is given in Table 4.3. These dimensions correspond to those described in Figure 3.1. The results for the above operating conditions are given in Table 4.4.

Table 4.1 Design information for the APTMS PAO-Air heat exchanger.

	Cold Fluid	Hot Fluid
Fluid Type	Air	PAO
Design Inlet Temperature (K)	284.45	321.56
Design Flow Rate (kg/s)	5.1021	1.8144
Design Heat Load (W)	122,260	

Table 4.2 Design information for FTMS PAO-Air heat exchanger.

	Cold Fluid	Hot Fluid
Fluid Type	PAO	JP8
Design Inlet Temperature (K)	287.57	294.79
Design Flow Rate (kg/s)	3.63	13.99
Design Heat Load (W)	50,000	

Table 4.3 Geometry parameters used for model validation

	s_1	h_1	l_1	t_{f1}	t_1	s_2	h_2	l_2	t_{f2}	t_2	L
	mm	mm	mm	mm	mm	mm	mm	mm	mm	mm	m
APTMS Exchanger	1.5	10.6	6.3	0.208	11.361	0.83	10.6	6.35	0.472	15.313	0.841
FTMS Exchanger	0.836	10.6	6.299	0.322	14.29	0.83	10.6	6.35	0.462	17.686	0.38

Table 4.4 Heat exchanger validation results.

	Weise	Current Model	Percent Difference
APTMS HX Mass (kg)	290.7	229.0	21.2
FTMS HX Mass (kg)	404.3	542.3	25.4

For both the APTMS PAO-Air heat exchanger and the FTMS PAO-FUEL heat exchanger, the difference between the data from Weise and the current model was less than 26%. This difference is found to be reasonable given the modifications made to Weise's model and the differing correlations used for such items as the Nusselt number. For this model, a modification was made to the pressure drop correlation originally used in Weise[5]. This resulted in the pressure drops generated by this model to be lower than those generated in Weise. Another difference between this model and Weise was that the convergence criteria used for the fluid area was changed. In Weise, the model was said to be converged when the fluid area of either the hot or the cold side met the convergence criteria of a difference of $1x10^{-5}$ between iterations. For this model, the criteria was changed so that the area of both the hot and cold sides had to meet the convergence criteria. Both of these changes account for differences seen between this work's model and Weise's[5].

Further validation is seen in the results from Section 4.4 where the variable fin data is tabulated. According to Williams[20], research has shown that microchannel based metallic heat exchangers could potentially offer 20-30% weight reduction over the state-of-the-art compact plate-fin heat exchangers. For the variable fin efficiency heat exchangers, this trend is also observed using the microchannel model developed in this thesis. This is a partial validation of

the data generated by the microchannel heat exchanger model indicating that it is within reasonable bounds.

4.2 Fixed-Fin-Efficiency APTMS PAO-Air Microchannel Heat Exchanger

The microchannel model developed here can be used to generate design parameter values for any combination of physically reasonable operational parameter values including those for the mass flow rates on both sides, the fluid temperatures on both sides, and the heat load that need to be handled by the exchanger. By varying these parameter values, a better understanding of the behavior of the microchannel heat exchanger can be developed.

4.2.1 Accounting for Fin Geometry with a Fixed Fin Efficiency

Previous work done by Gvozdich[4] and Weise[6] use the assumption that the fin efficiency for the hot- and cold- side fins is 0.7 regardless of geometry. This assumption removes the equality constraints seen in Table 3.5 for the fin efficiency given a fin geometry. In order to determine the validity of this assumption, an APTMS compact plate-fin and a microchannel heat exchanger are sized without this constraint. The fin efficiency obtained using this optimization is then compared to the assumption of 0.7 to determine if this is valid.

As can be seen in Figures 4.1 to 4.4, using the assumption that $\eta = 0.7$ without taking into account fin geometry is an underestimation of the fin efficiency on the hot side of the heat exchangers (Figures 4.2 and 4.4) while it is an overestimation on the cold side (Figures 4.1 and 4.3). The reason for the difference in the trends on the hot and the cold sides is primarily due to the differences between the hot side and cold side working fluids. For this study, PAO is used as the hot fluid while air is used as the cold fluid. These fluids have vastly different thermal conductivities, densities, and viscosities. This results in a difference in the convective heat transfer coefficient, which is an integral part of the fin efficiency equation seen in Table 3.5. Higher convective heat transfer coefficients result in lower fin efficiencies, accounting for the differences seen in Figures 4.1 to 4.4.

Because of the differences seen, a new model is developed taking into account the fact that the fin geometry should be constrained by the fin efficiency if a fin efficiency is to be assumed. In order to do this, the fin length, L_{fin}, is determined using the fin efficiency correlation seen in Table 3.5. The fin strip length, l, and the fin thickness, t_f, are kept as optimization decision

variables. The differences in masses between these two models for a microchannel heat exchanger are shown in Figures 4.5 and 4.6. It was found that the difference at each heat load between the two masses was 1.7±0.2 kg. This results in the monotonically decreasing percent difference seen in Figure 4.6 because as heat load increases, the mass of the heat exchanger must also increase. This results in the 1.7 kg difference being a smaller and smaller percent of the overall mass. Due to the inaccuracy of using the previously made assumption, it was determined that the new fixed efficiency model taking into account fin geometry would be used for all other studies in this research.

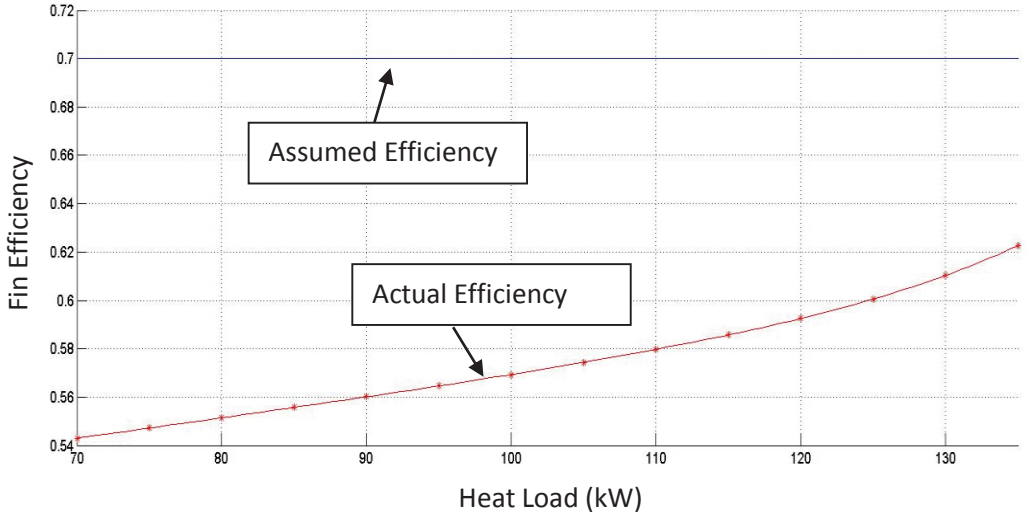

Figure 4.1 APTMS cold side microchannel heat exchanger actual vs assumed fin efficiency.

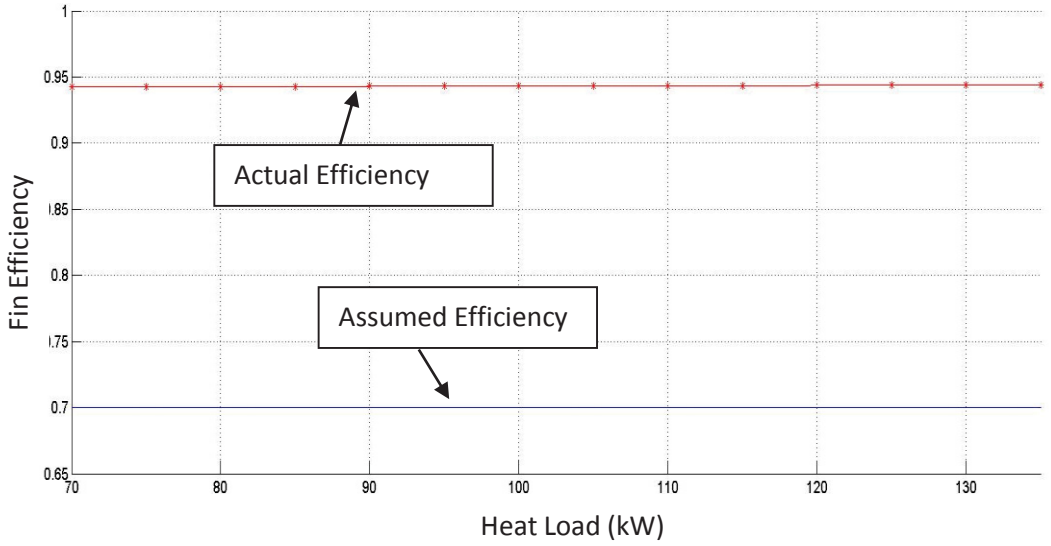

Figure 4.2 APTMS hot side microchannel heat exchanger actual vs assumed fin efficiency.

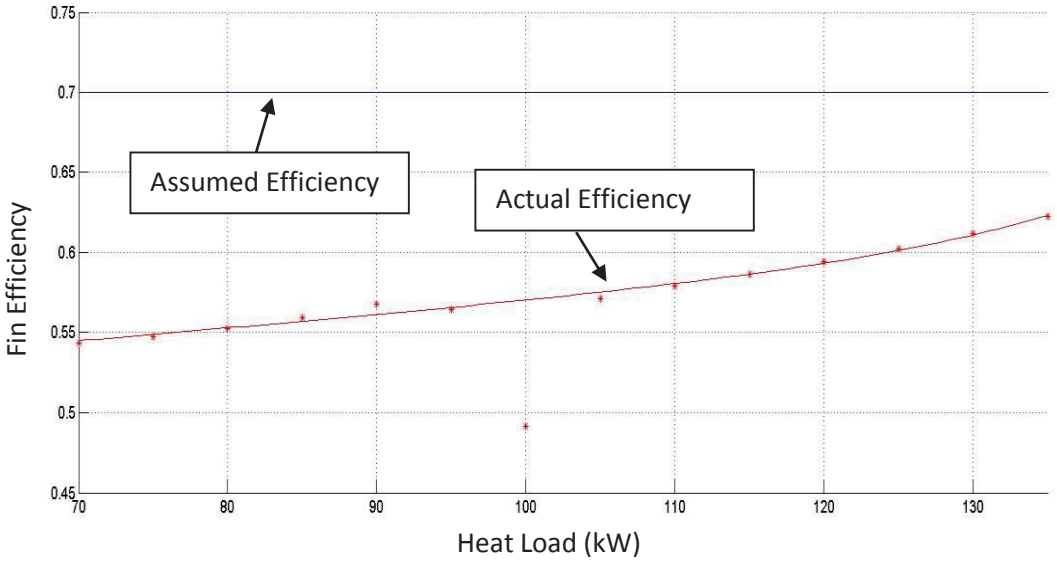

Figure 4.3 APTMS cold side plate fin heat exchanger actual vs assumed fin efficiency.

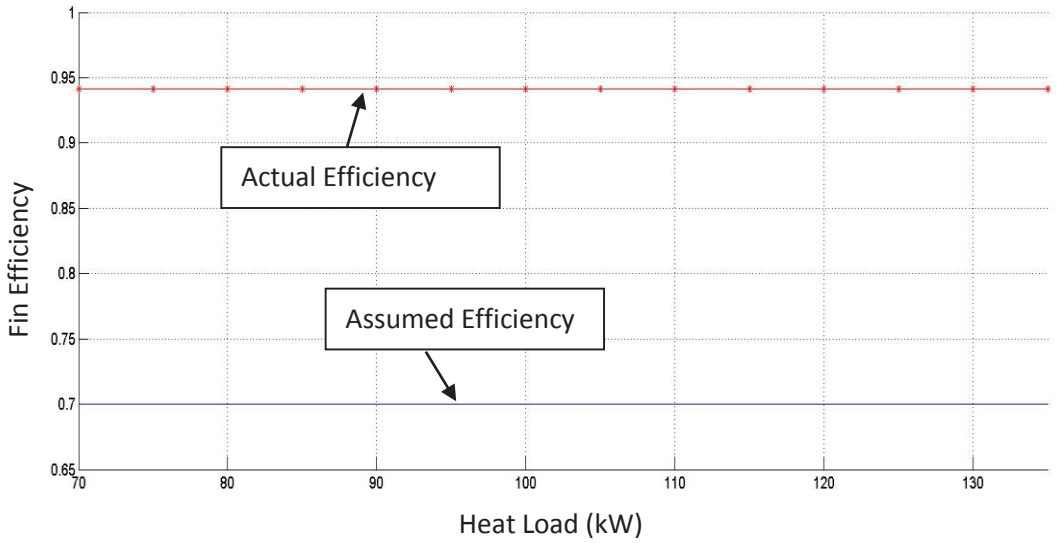

Figure 4.4 APTMS hot side plate fin heat exchanger actual vs assumed fin efficiency.

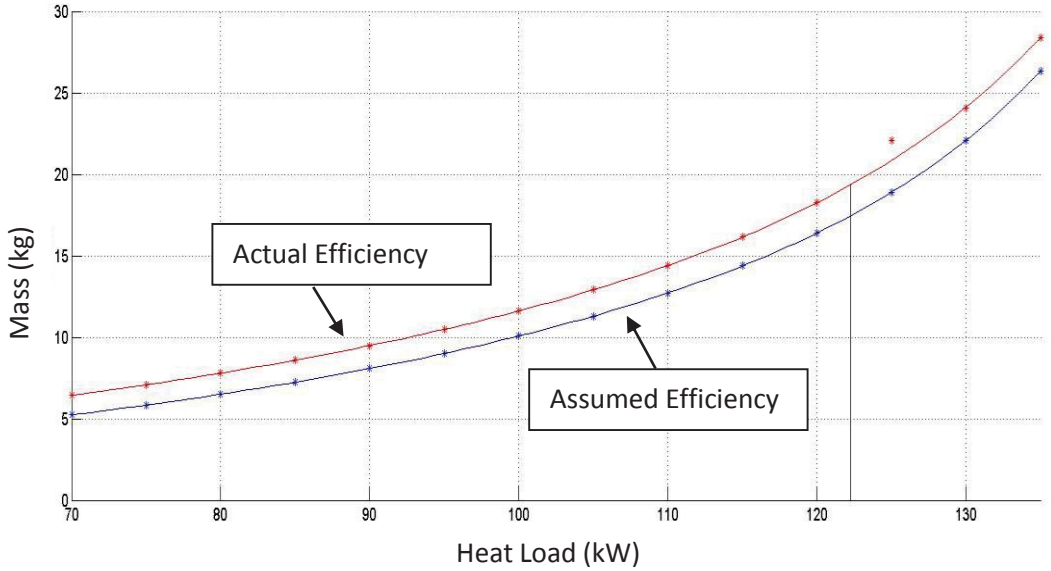

Figure 4.5 APTMS microchannel heat exchanger mass with actual vs assumed fin efficiency.

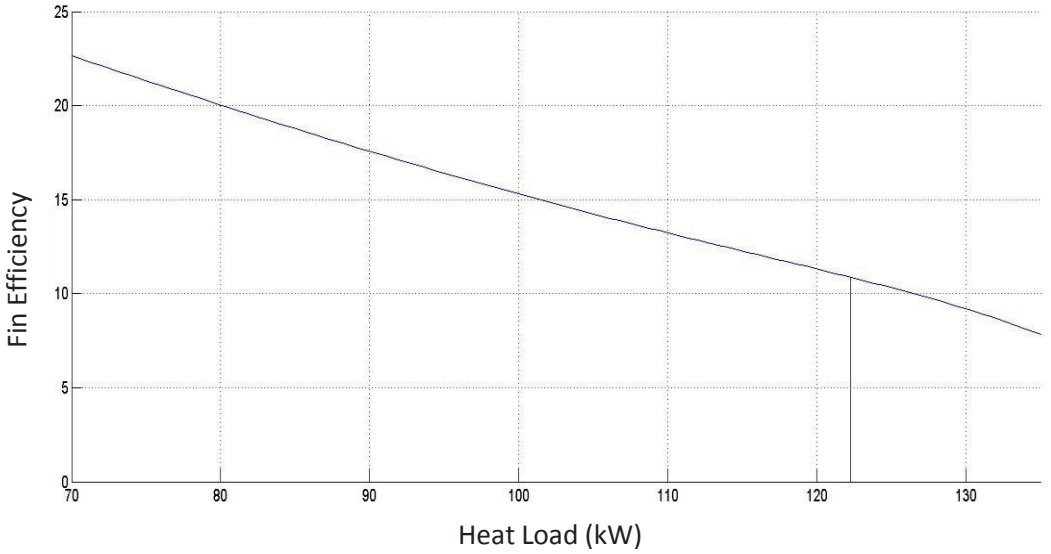

Figure 4.6 APTMS microchannel heat exchanger mass percent increase with actual vs assumed fin efficiency.

4.2.2 Fixed-Fin-Efficiency APTMS Heat Exchangers using the New Fin-Efficiency-Geometry Constraint

The mass trend of a microchannel heat exchanger sized for APTMS operating parameter values versus a plate fin heat exchanger sized to the same parameter values is shown in Figure 4.7 versus a varying heat load. As can be seen in this figure, the mass needed for the given mass

flow rates and inlet temperatures for a microchannel APTMS PAO-Air heat exchanger is lower than that of a similarly sized compact plate-fin heat exchanger for a range of heat loads varying from 70 to 135 kW. This trend is further exhibited in Figure 4.8 which shows the percentage drop in mass from the compact plate fin heat exchanger to the microchannel heat exchanger ranging from about 28% at the low heat load to 54% at the high heat load. At the design heat load for the APTMS, this results in reduction of approximately 45% in mass or 16 kg.

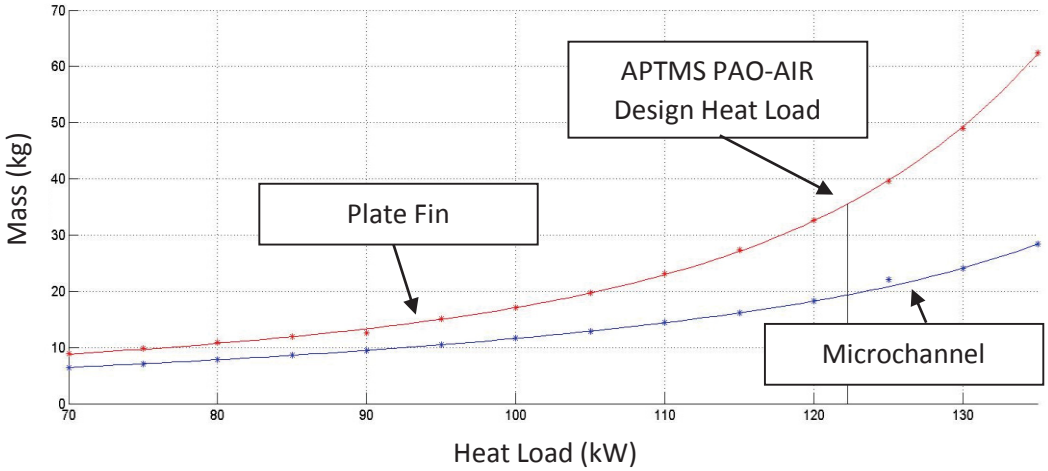

Figure 4.7 APTMS heat exchanger mass versus heat load for a compact plate fin and microchannel heat exchanger.

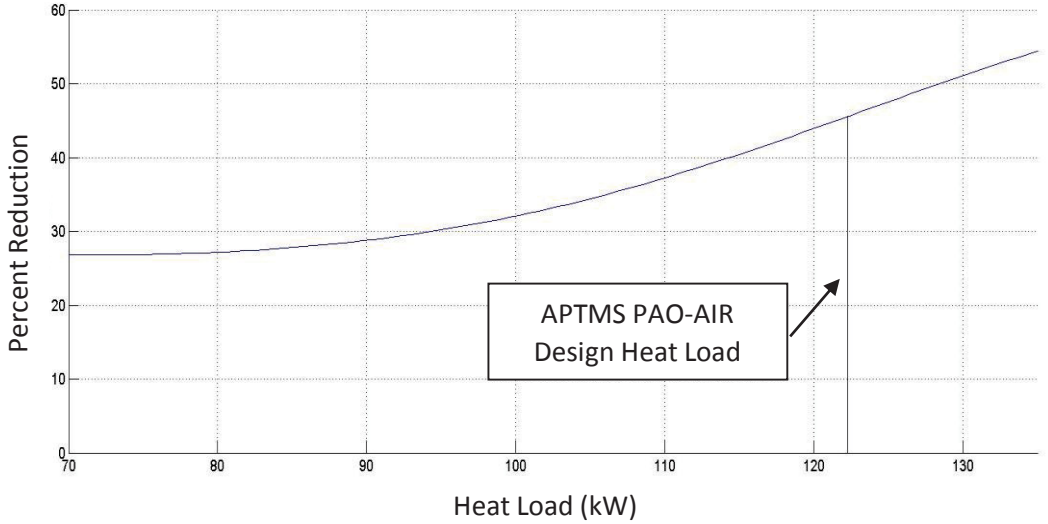

Figure 4.8 Percent reduction in APTMS heat exchanger mass for a compact plate fin and a microchannel heat exchanger

For the APTMS heat exchanger, this reduction in mass can be attributed to several factors. First of all, the heat transfer coefficient from the working fluid to the fins increases with reduced hydraulic diameter. Since the microchannel heat exchanger has a significantly smaller hydraulic diameter at each heat load, its heat transfer performance is boosted, allowing it to transfer more heat from one working fluid to the other with less fluid volume and, therefore, less overall mass. This hydraulic diameter trend is seen in Figures 4.9 and 4.10 for the cold and hot sides of the APTMS heat exchanger. It can also be from these figures that the difference in the hydraulic diameter between the microchannel and plate-fin heat exchangers gets larger with increasing heat load. This is the cause of the increase in percent mass reduction with increasing heat load seen in Figure 4.8.

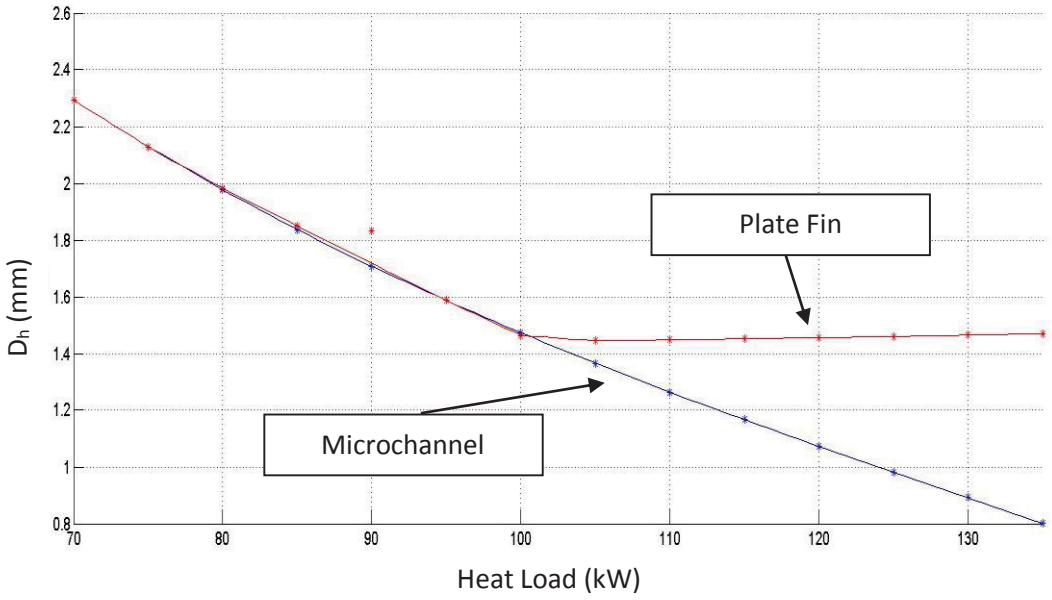

Figure 4.9 Cold side hydraulic diameter of a microchannel and compact plate fin heat exchanger sized for the APTMS tip-to-tail Loads

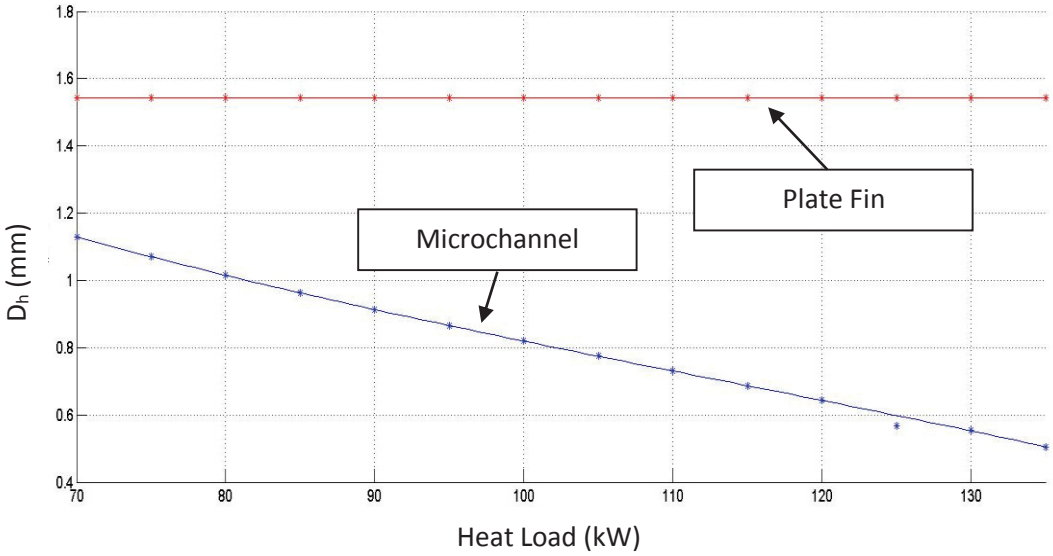

Figure 4.10 Hot side hydraulic diameter of a microchannel and compact plate fin heat exchanger sized for the APTMS tip-to-tail loads

It can be seen in Figures 4.9 and 4.10 that the plate-fin heat exchanger's hydraulic diameter plateaus at approximately 1.5 mm. This plateau is seen for all heat loads on the hot side and above 100kW on the cold side. The reason for this plateau is that during the optimization process, all of the optimization decision variables for both the microchannel and plate-fin heat exchangers trend towards either the upper or lower bounds placed upon them. Furthermore, it was found that for the heat loads and operational parameter values used only the fin channel width, $s_{1,2}$, fin channel height, $h_{1,2}$, and the overall length of the exchanger, L, do not go to their bound. Tables 4.5 and 4.6 contain the data for the optimization parameters that exhibit this trend. In these tables it can be seen that the fin strip length, $l_{1,2}$, is consistently at its upper bound of 6.35 mm while the fin thickness, $t_{f1,2}$ and plate thickness, $t_{1,2}$, go to their lower bound of 0.15 mm and 0.5 mm respectively. The fin channel width and height varies with heat load, with the fin channel width trending towards its lower bound of 0.2 mm for the microchannel heat exchanger and 0.83 mm for the compact plate fin heat exchanger. The fin channel height shown in these tables is derived from the fin efficiency constraint described in *Section* 4.2.1. It can clearly be seen that the plateau of hydraulic diameter seen in the plate-fin compact heat exchanger corresponds to the fact that unlike the microchannel heat exchanger, the fin channel width of the plate-fin heat exchanger reaches its lower bound in the heat loads that were used.

Table 4.5 APTMS microchannel heat exchanger optimal geometries

Heat Load	s_1	h_1	l_1	t_{f1}	t_1	s_2	h_2	l_2	t_{f2}	t_2	L
kW	**mm**	**mm**	**mm**	**mm**	**mm**	**mm**	**mm**	**mm**	**mm**	**mm**	**m**
70	1.46	5.98	6.35	0.15	0.50	0.60	13.34	6.35	0.15	0.50	0.10
75	1.32	6.06	6.35	0.15	0.50	0.57	12.94	6.35	0.15	0.50	0.10
80	1.21	6.15	6.35	0.15	0.50	0.54	12.57	6.35	0.15	0.50	0.10
85	1.10	6.24	6.35	0.15	0.50	0.51	12.21	6.35	0.15	0.50	0.10
90	1.01	6.34	6.35	0.15	0.50	0.49	11.86	6.35	0.15	0.50	0.10
95	0.93	6.43	6.35	0.15	0.50	0.46	11.52	6.35	0.15	0.50	0.10
100	0.85	6.54	6.35	0.15	0.50	0.44	11.18	6.35	0.15	0.50	0.10
105	0.78	6.66	6.35	0.15	0.50	0.41	10.84	6.35	0.15	0.50	0.10
110	0.71	6.79	6.35	0.15	0.50	0.39	10.50	6.35	0.15	0.50	0.10
115	0.65	6.93	6.35	0.15	0.50	0.36	10.16	6.35	0.15	0.50	0.10
120	0.59	7.10	6.35	0.15	0.50	0.34	9.81	6.35	0.15	0.50	0.10
125	0.54	7.30	6.35	0.15	0.50	0.76	7.68	6.35	0.15	0.50	0.10
130	0.49	7.55	6.35	0.15	0.50	0.29	9.05	6.35	0.15	0.50	0.10
135	0.43	7.88	6.35	0.15	0.50	0.27	8.63	6.35	0.15	0.50	0.10

Table 4.6 APTMS plate fin heat exchanger optimal geometries

Heat Load	s_1	h_1	l_1	t_{f1}	t_1	s_2	h_2	l_2	t_{f2}	t_2	L
kW	**mm**	**mm**	**mm**	**mm**	**mm**	**mm**	**mm**	**mm**	**mm**	**mm**	**m**
70	1.46	5.98	6.35	0.15	0.90	0.83	15.91	6.35	0.15	0.90	0.10
75	1.32	6.06	6.35	0.15	0.90	0.83	15.91	6.35	0.15	0.90	0.10
80	1.21	6.15	6.35	0.15	0.90	0.83	15.91	6.35	0.15	0.90	0.10
85	1.11	6.23	6.35	0.15	0.90	0.83	15.91	6.35	0.15	0.90	0.10
90	1.10	6.24	6.35	0.15	0.90	0.83	15.91	6.35	0.15	0.90	0.10
95	0.93	6.43	6.35	0.15	0.90	0.83	15.91	6.35	0.15	0.90	0.10
100	0.84	6.55	6.35	0.15	0.90	0.83	15.91	6.35	0.15	0.90	0.10
105	0.83	6.69	6.35	0.15	0.90	0.83	15.91	6.35	0.15	0.90	0.11
110	0.83	6.85	6.35	0.15	0.90	0.83	15.91	6.35	0.15	0.90	0.12
115	0.83	7.02	6.35	0.15	0.90	0.83	15.91	6.35	0.15	0.90	0.14
120	0.83	7.21	6.35	0.15	0.90	0.83	15.91	6.35	0.15	0.90	0.15
125	0.83	7.42	6.35	0.15	0.90	0.83	15.91	6.35	0.15	0.90	0.17
130	0.83	7.67	6.35	0.15	0.90	0.83	15.91	6.35	0.15	0.90	0.20
135	0.83	7.96	6.35	0.15	0.90	0.83	15.91	6.35	0.15	0.90	0.24

It can be seen Figure 4.11 that the plate-fin heat exchanger's overall length, L, begins to rise even more steadily above a heat load of 100 kW. This rise also corresponds to the fin channel width plateauing at its lowest constrained value of 0.83 mm. This is important as the overall length of the heat exchanger has a direct impact on the mass curve for that heat exchanger. As seen in Figure 4.7, above approximately a 100 kW heat load, the slope of the mass curve for the plate-fin heat exchanger increases at a high rate. This increase is directly related to the increase in overall length seen in Figure 4.11.

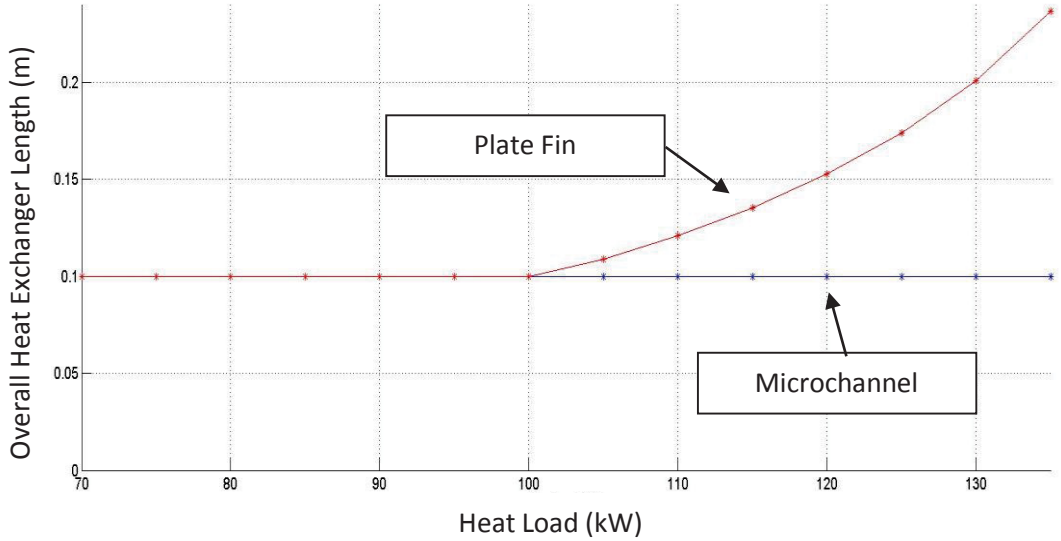

Figure 4.11 Overall heat exchanger length for APTMS microchannel vs plate fin heat exchanger

One factor that limits microchannel heat exchanger performance is the pressure drop across the heat exchanger. It can be seen in Figure 4.12 seen that the pressure drop of the optimally sized microchannel heat exchanger goes to the constraint of 30 kPa at all heat loads. This pressure drop is consistently higher than the pressure drops of the plate-fin heat exchanger. The difference is due to the lower hydraulic diameter seen in the microchannel heat exchanger which cause a direct increase in the pressure drop as seen in the correlation from Table 3.2. Because of this, a balance must be obtained between the pumping power needs of the TMS system and the benefits in thermal performance afforded by the use of microchannel heat exchangers.

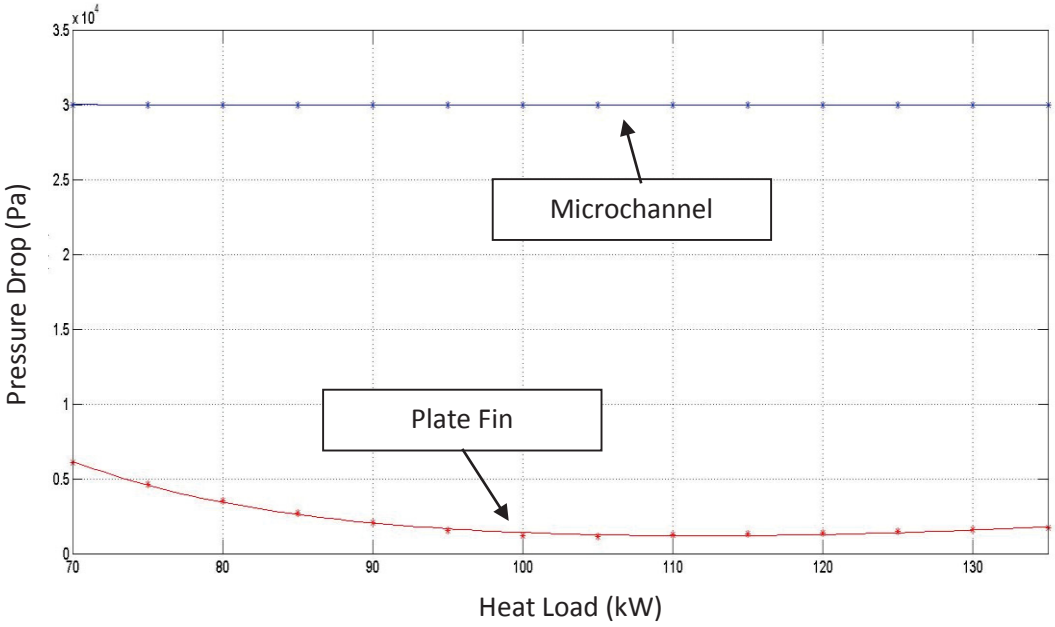

Figure 4.12 APTMS pressure drop for microchannel vs plate-fin heat exchanger.

4.3 Fixed-Fin-Efficiency FTMS PAO-Fuel Microchannel Heat Exchanger using New Fin-Efficiency-Geometry Constraint

It can be seen in Figure 4.13 that the mass trend for the FTMS heat exchangers follows the same trend as that for the APTMS heat exchangers. Similar to the APTMS heat exchangers, the liquid-liquid FTMS heat exchangers follow a trend where the microchannel heat exchanger has a consistently lower weight than the compact plate-fin heat exchanger. This is further evidenced in Figure 4.14 which depicts the percent mass reduction between the FTMS plate-fin heat exchanger and the microchannel heat exchanger. It should be noted that the heat loads used for the FTMS heat exchangers are lower than those used for the APTMS heat exchangers. This is due to the differences in the heat loads placed on the FTMS system in the tip-to-tail model.

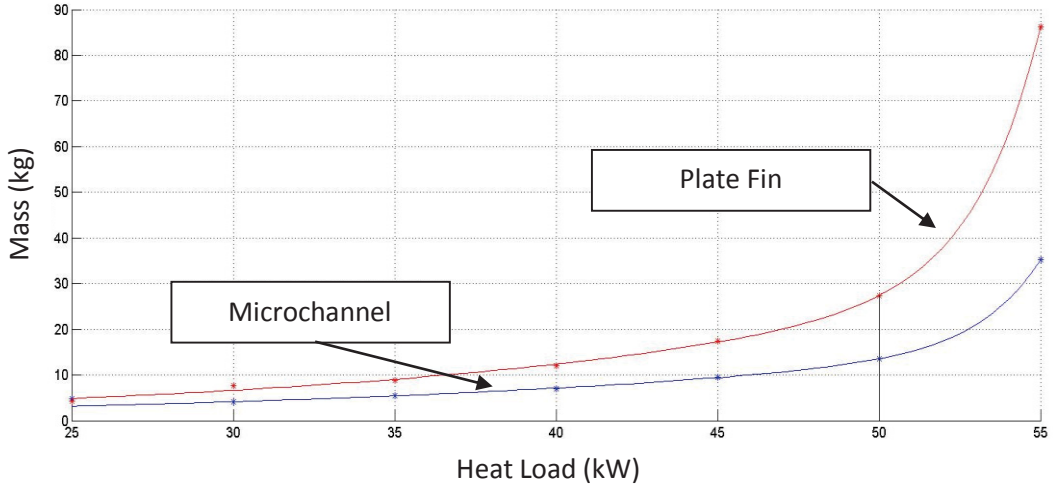

Figure 4.13 FTMS heat exchanger mass versus heat load for a compact plate fin and microchannel heat exchanger.

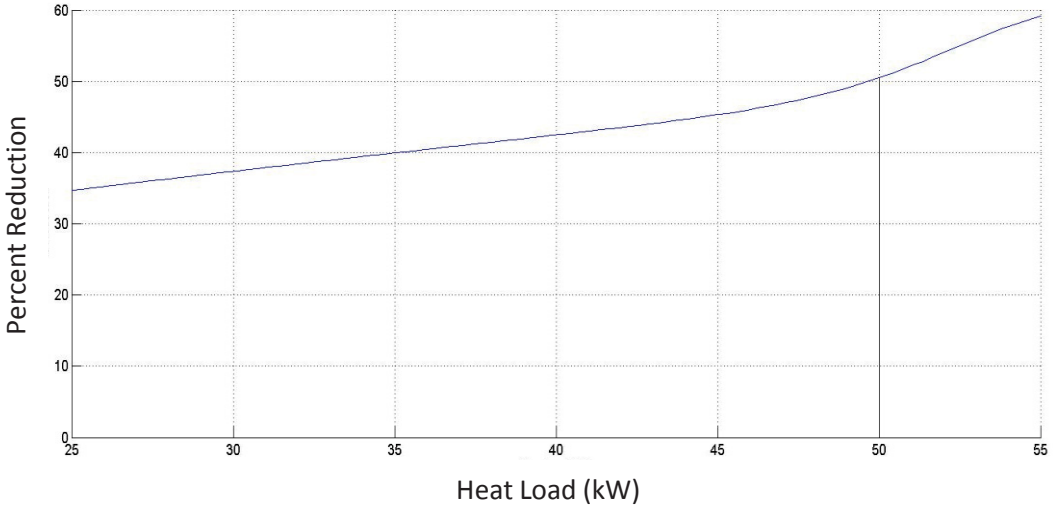

Figure 4.14 Percent reduction in FTMS heat exchanger mass for a compact plate fin and a microchannel heat exchanger

As is seen in Figures 4.13 and 4.14 the percent reduction in mass between the compact plate-fin heat exchanger and the microchannel heat exchanger varies between approximately 34 to 60%. This is similar to the trend seen in the APTMS heat exchanger studies and can again be attributed to differences in the hydraulic diameter between the microchannel and plate-fin heat exchangers. As evidenced by Figures 4.15 and 4.16 the microchannel heat exchanger consistently has a lower hydraulic diameter on both the hot and cold sides. This results in better

heat transfer and, therefore, a lower mass needed to dissipate the same heat load as a larger compact plate-fin heat exchanger.

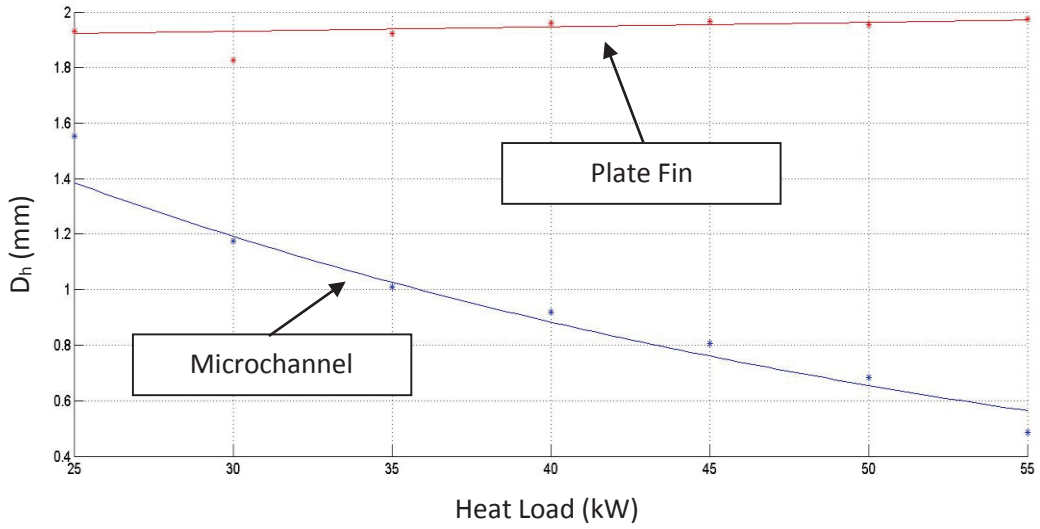

Figure 4.15 Cold side hydraulic diameter of a microchannel and compact plate fin heat exchanger sized for the FTMS tip-to-tail loads

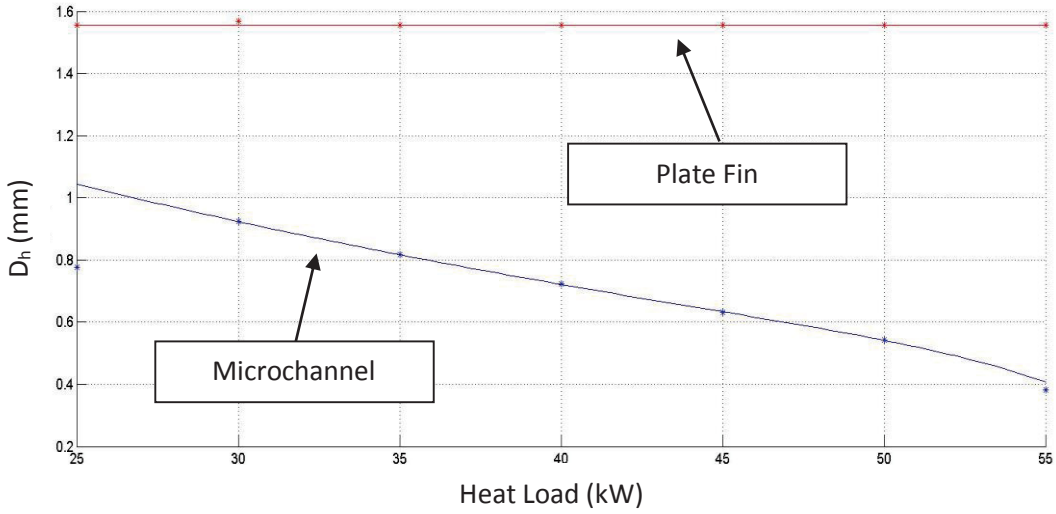

Figure 4.16 Hot side hydraulic diameter of a microchannel and compact plate-fin heat exchanger sized for the FTMS tip-to-tail loads

The FTMS microchannel heat exchanger results also exhibited the same trend in l, t_f, and t seen in the APTMS heat exchanger results. Each of these design decision variables went to their bounds, while the fin channel width, s, and height, h, varied with the heat load. This trend is

exhibited in Tables 4.7 and 4.8. Similar to the APTMS results, in these tables it can be seen that the fin strip length, $l_{1,2}$, is consistently at its upper bound of 6.35 mm while the fin thickness, $t_{f1,2}$ and plate thickness, $t_{1,2,}$ go to their lower bound of 0.15 mm and 0.5 mm respectively for the microchannel heat exchanger and 0.15 mm and 0.9 mm for the plate-fin heat exchanger. The fin channel width and height varies with heat load, with the fin channel width trending towards its lower bound of 0.2 mm for the microchannel heat exchanger and 0.83 mm for the compact plate fin heat exchanger. The fin channel height shown in these tables is derived from the fin efficiency constraint described in *Section* 4.2.1. It can again be seen that the plateau of hydraulic diameter seen in the plate-fin compact heat exchanger corresponds to the fact that unlike the microchannel heat exchanger, the fin channel width of the plate-fin heat exchanger reaches its lower bound in the heat loads that were used.

Table 4.7 FTMS microchannel heat exchanger optimal geometries

Heat Load	s_1	h_1	l_1	t_{f1}	t_1	s_2	h_2	l_2	t_{f2}	t_2	L
kW	**mm**	**mm**	**mm**	**mm**	**mm**	**mm**	**mm**	**mm**	**mm**	**mm**	**m**
25	0.84	16.00	6.35	0.15	0.50	0.41	13.02	6.35	0.15	0.50	0.10
30	0.63	13.70	6.35	0.15	0.50	0.49	14.28	6.35	0.15	0.50	0.10
35	0.54	12.59	6.35	0.15	0.50	0.43	13.36	6.35	0.15	0.50	0.10
40	0.49	11.97	6.35	0.15	0.50	0.38	12.52	6.35	0.15	0.50	0.10
45	0.43	11.13	6.35	0.15	0.50	0.33	11.66	6.35	0.15	0.50	0.10
50	0.36	10.18	6.35	0.15	0.50	0.28	10.75	6.35	0.15	0.50	0.10
55	0.26	8.50	6.35	0.15	0.50	0.20	8.97	6.35	0.15	0.50	0.11

Table 4.8 FTMS plate fin heat exchanger optimal geometries

Heat Load	s_1	h_1	l_1	t_{f1}	t_1	s_2	h_2	l_2	t_{f2}	t_2	L
kW	**mm**	**mm**	**mm**	**mm**	**mm**	**mm**	**mm**	**mm**	**mm**	**mm**	**m**
25	1.04	18.20	6.35	0.15	0.90	0.83	19.05	6.35	0.15	0.90	0.18
30	1.03	19.03	2.43	0.19	0.93	0.84	19.12	6.02	0.15	0.92	0.20
35	1.04	18.16	6.35	0.15	0.91	0.83	19.03	6.30	0.15	0.90	0.26
40	1.06	18.37	6.35	0.15	0.90	0.83	19.00	6.35	0.15	0.90	0.32
45	1.06	18.39	6.35	0.15	0.90	0.83	19.00	6.35	0.15	0.90	0.40
50	1.06	18.34	6.35	0.15	0.90	0.83	19.00	6.35	0.15	0.90	0.51
55	1.07	18.45	6.35	0.15	0.90	0.83	19.00	6.35	0.15	0.90	0.97

It is also again seen in the FTMS liquid-liquid heat exchanger that the overall length is one of the main factors impacting the mass. In the case of the FTMS plate-fin heat exchanger, at all heat loads examined the hydraulic diameter, D_h, of the exchanger ducts has settled on the lowest possible value (See Figures 4.15 and 4.16). In order to compensate for this, the length of the heat exchanger, L, must be increased to handle higher heat loads. This trend is seen in Figure 4.17. This increase in the overall length is a key factor in the rapid increase in the mass curve seen in Figure 4.13. The increase in length of the plate-fin heat exchanger is in contrast to the microchannel heat exchanger length which remains at its lower bound of 0.1 m for almost all heat loads analyzed. The reason for this contrast is that the hydraulic diameter of the microchannel heat exchanger is still decreasing after the plate-fin heat exchanger's hydraulic diameter has plateaued. This allows the microchannel heat exchanger to maintain a higher heat transfer rate than the plate-fin heat exchanger at a shorter overall length.

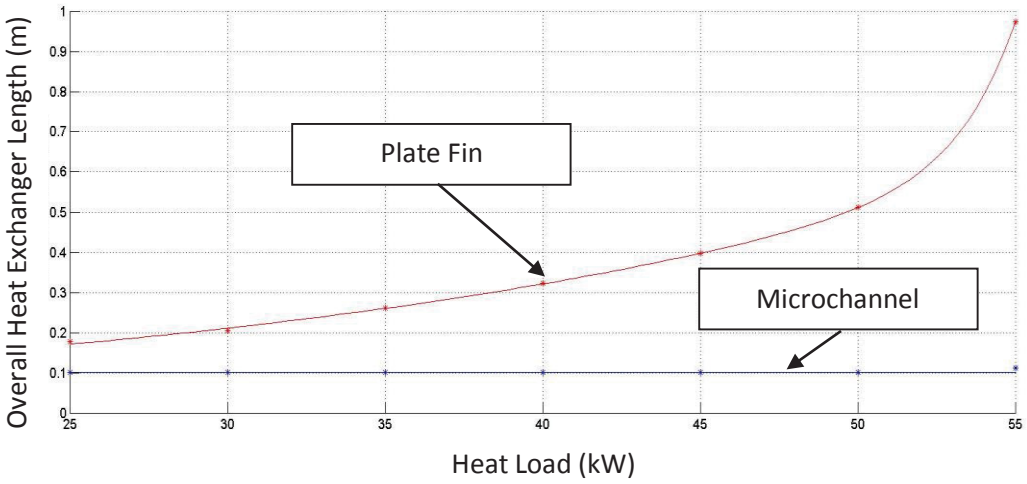

Figure 4.17 Overall heat exchanger length for APTMS microchannel and plate-fin heat exchangers

4.4 Variable-Fin-Efficiency APTMS PAO-Air Microchannel Heat Exchanger

Previous work done makes the assumption that the fin efficiency used in the models is fixed at 0.7. Because of this, a study on the impact of having a varying fin efficiency is conducted. The results of this study are presented below.

Figures 4.18 and 4.19 demonstrate the mass trend for a microchannel and plate-fin heat exchanger with both fixed and variable fin efficiencies. For the microchannel heat exchanger the

percent difference between the variable and fixed efficiency models is 1.58±3%. For the plate-fin heat exchanger the percent difference between the variable and fixed efficiency models is 2.3±2%. However, since the differences are so small and the uncertainty in the optimization results sufficiently high, there is no significant difference in the results.

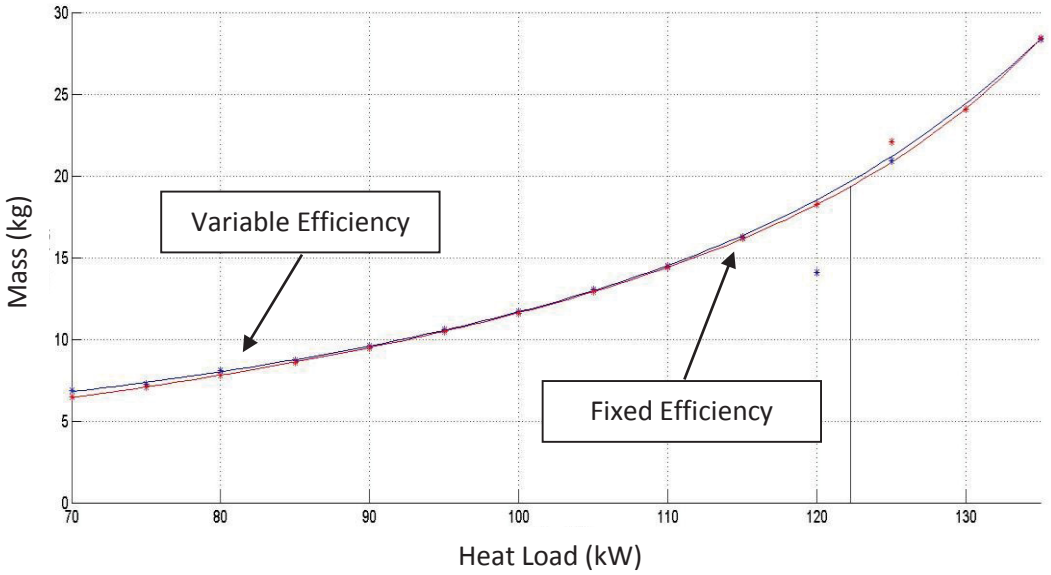

Figure 4.18 Mass trend of an APTMS microchannel heat exchanger using both a fixed and variable fin efficiency

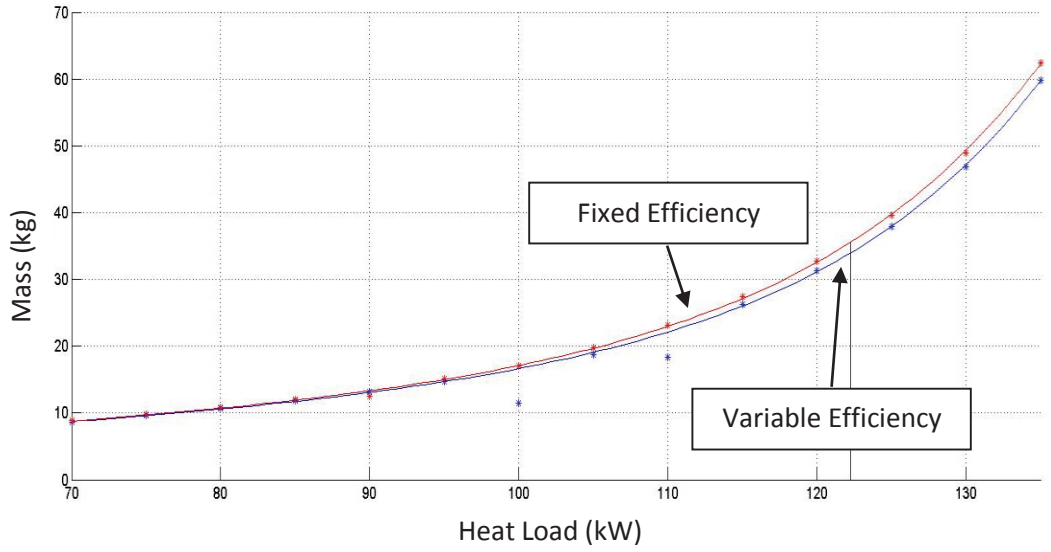

Figure 4.19 Mass trend of an APTMS plate fin heat exchanger using both a fixed and variable fin efficiency

The fin efficiencies for the microchannel and plate-fin heat exchangers is given in Figures 4.20 to 4.23. It can be seen from these plots that on the cold side, the fin efficiencies settle to values close to the 0.7 value assumed in the fixed efficiency model. However, on the hot side the fin efficiencies are higher than the assumed value of 0.7. However, these differences are not drastic enough to cause a large deviation in the mass between the fixed and variable fin efficiencies. The overall effect is that the difference in the variable fin model versus the plate fin model is small enough that using the less complicated fixed fin efficiency approach in the design optimization of the heat exchanger would be perfectly acceptable.

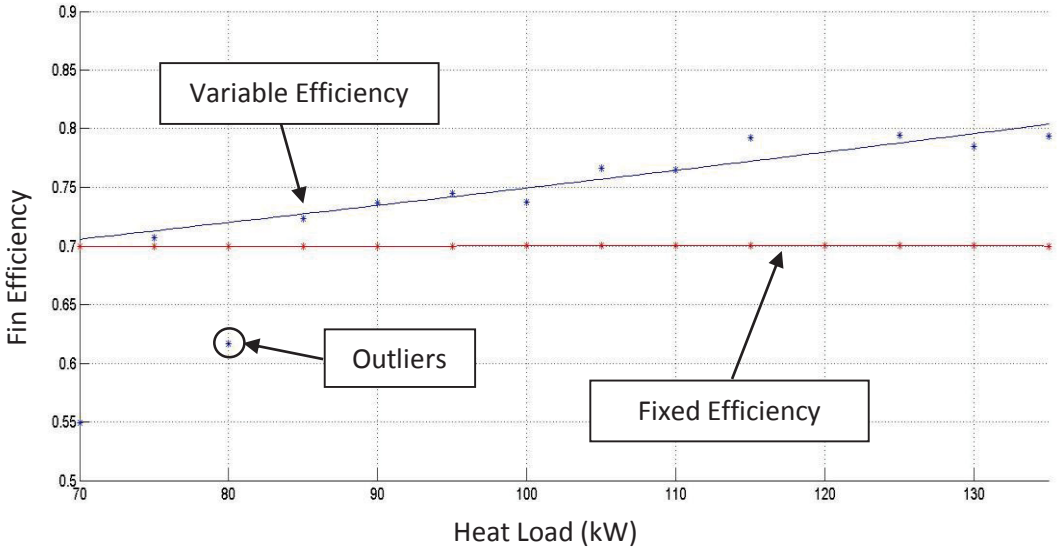

Figure 4.20 Microchannel heat exchanger fin efficiency cold side.

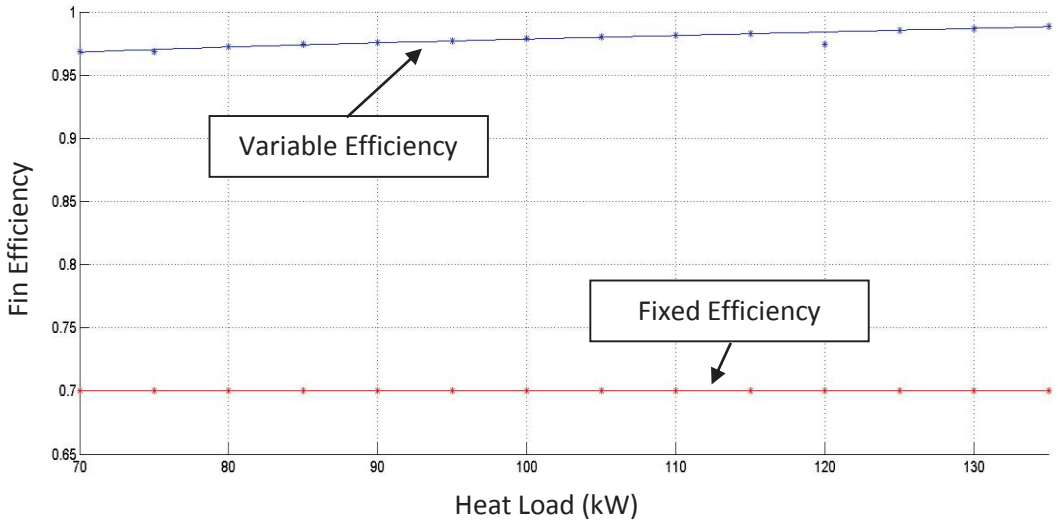

Figure 4.21 Microchannel heat exchanger fin efficiency hot side.

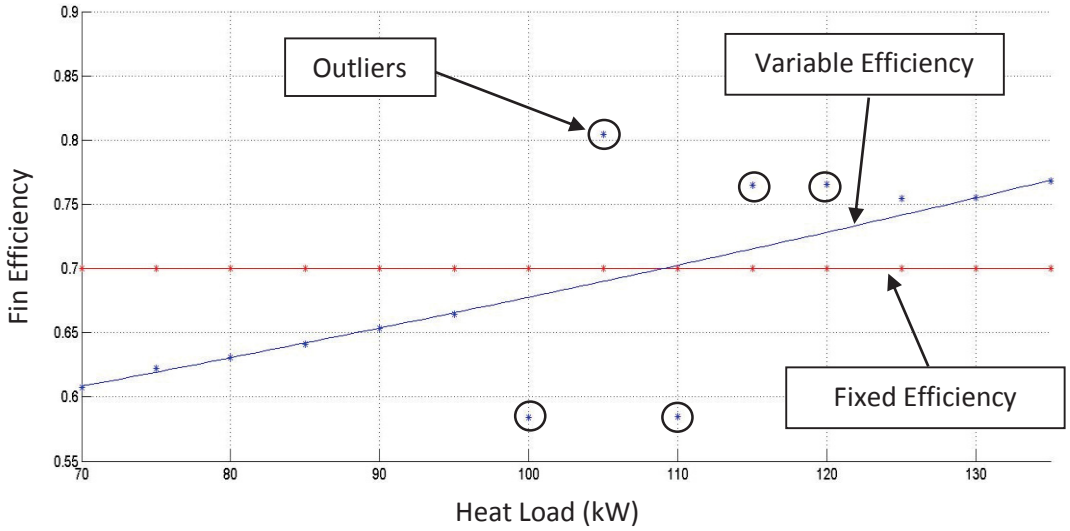

Figure 4.22 Plate-fin heat exchanger efficiency cold side.

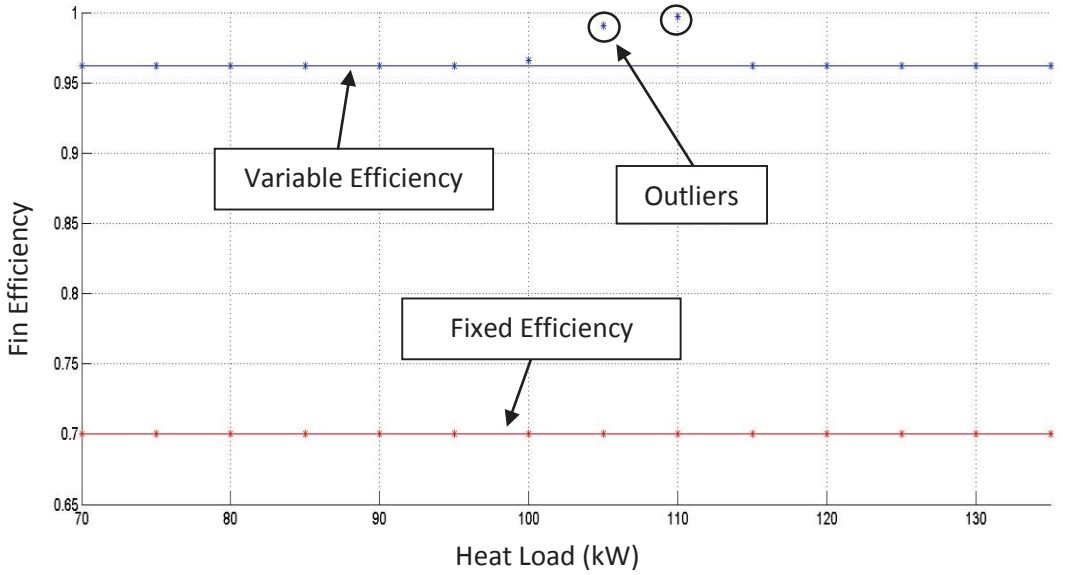

Figure 4.23 Plate-fin heat exchanger efficiency hot side

One other aspect of the variable versus fixed fin efficiency is the convergence of the optimization of the two models. For the fixed-fin-efficiency model, using a gradient-based optimization method produces smooth curves without a lot of outliers (local optimums) from the curve. However, the variable-fin-efficiency model produces more outliers to the curve fits and takes longer to converge on a solution. Because of this and the fact that the mass curve difference

between the two models is small, it can be concluded that the fixed-fin efficiency assumption and can be used to improve model performance with negligible loss to the final results of the design process.

4.5 Phase Change Materials

Three different phase change materials (PCMs) were utilized in the PCES model described in *Section* 3.3 and the results are given below. These materials are chosen due to their similar densities and for their melting temperatures at or below the working fluid temperature of 300 K. This fluid temperature is taken out of Gvozdich[4] as being representative of the fluid temperature seen in a DEW TMS. Table 4.9 contains values for the pertinent physical characteristics of these materials.

Table 4.9 Physical parameters of PCMs

		Pentadecane	Hexadecane	Octadecane
Melt Temperature	**°C**	10	18	27
Thermal Conductivity	**W/m/K**	0.2	0.15	0.15
Density	**kg/m^3**	768	770	800
Latent Heat of Fusion	**kJ/kg**	205	237	244

Due to the low thermal conductivities of these materials, Shanmugasundaram[22] proposes infusing them into K1100 carbon foam with a porosity of 0.8. By doing this, the effective thermal conductivity of the material can be raised. The results of this infusion are given in Table 4.10. Also, for the following simulation results and comparisons, three different thermal energy storage (TES) cell volumes are used. This was done to determine if the volume of the cells would have a significant impact on the results. The dimensions of these cells are given in Table 4.11. Using these volumes, the total mass of the PCM-Foam composite in the TES cell is determined, along with the mass of the PCM only and the energy storage capability of the PCM. This data is given in Table 4.12.

Table 4.10 Physical parameters of the PCM-carbon foam composite

		Pentadecane	Hexadecane	Octadecane
Effective Thermal Conductivity	**W/m/K**	220.16	165.12	165.12
Effective Density	**kg/m^3**	1054.4	1057.1	1098.3

Figure 4.11 TES Cell Volumes

		Small Cell	Medium Cell	Large Cell
Length Axial to Flow	**m**	0.5	1	2
Length Tangential to Flow	**m**	0.05	0.1	0.2
Depth	**m**	1	1	1
Total Volume	**m^3**	0.025	0.1	0.4

Table 4.12 Mass and energy stored of TES cells for different PCM's

		Pentadecane	Hexadecane	Octadecane
Total Composite Mass Small Cell	**kg**	26.36	26.43	27.46
Total Composite Mass Medium Cell	**kg**	105.44	105.71	109.83
Total Composite Mass Large Cell	**kg**	421.76	422.86	439.33
PCM Mass Small Cell	**kg**	15.36	15.4	16.0
PCM Mass Medium Cell	**kg**	61.44	61.6	64.0
PCM Mass Large Cell	**kg**	245.76	246.4	256.0
Energy Stored Small Cell	**kJ**	3148.8	3649.8	3904.0
Energy Stored Medium Cell	**kJ**	12595.2	14599.2	15616.0
Energy Stored Large Cell	**kJ**	50380.8	58396.8	62464.0

Based on the physical characteristics given in Tables 4.9 to 4.12, the differently sized PCM cells are modeled using a transient analysis. The temperature profile of these cells over time are given in Figures 4.24, 4.25, and 4.26. Given in Table 4.13 is the charge times for the various materials and volumes. The charge time is defined as the time for the phase change material to stabilize at the working fluid temperature of 300K, thus ending heat transfer out of the fluid. Out of the materials and volumes tested, the small volume pentadecane TES cell provides the closest performance to the 100 kW DEWS and TMS modeled in Gvozdich[4].

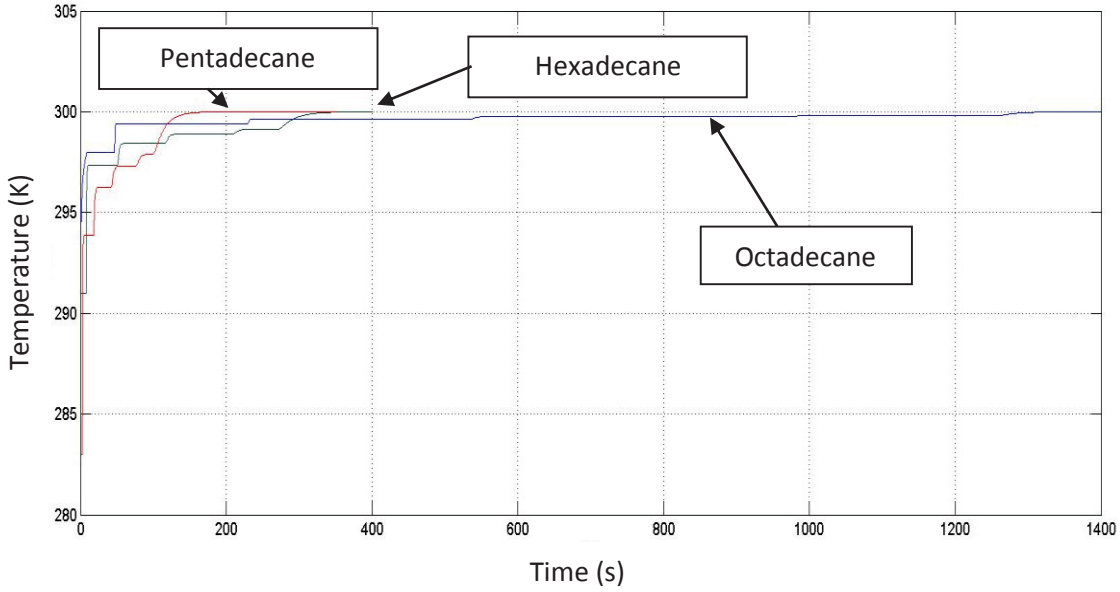

Figure 4.24 Temperature profile of a small volume TES cell for pentadecane, hexadecane, and octadecane.

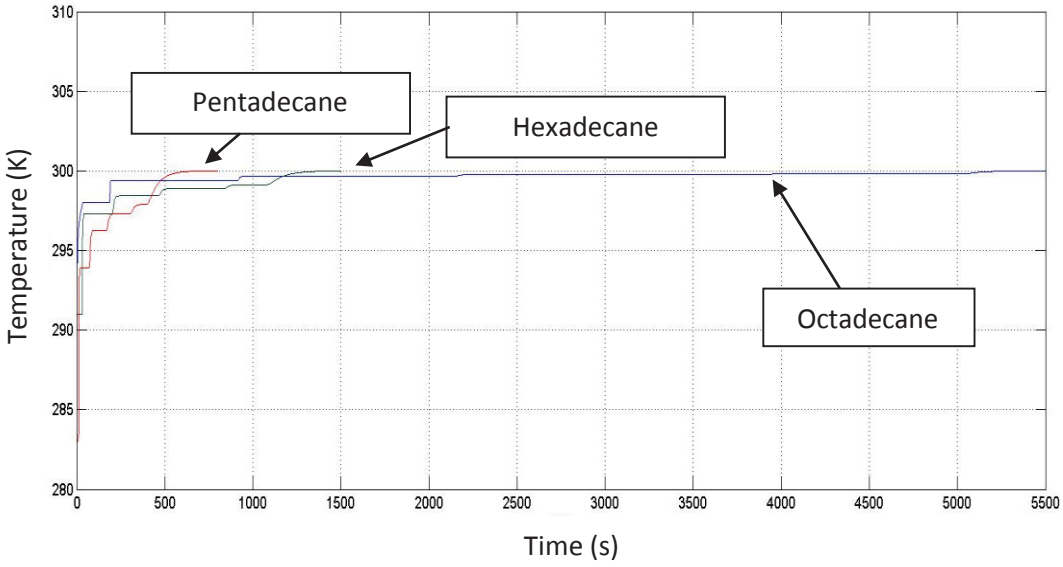

Figure 4.25 Temperature profile of a medium volume TES cell for pentadecane, hexadecane, and octadecane

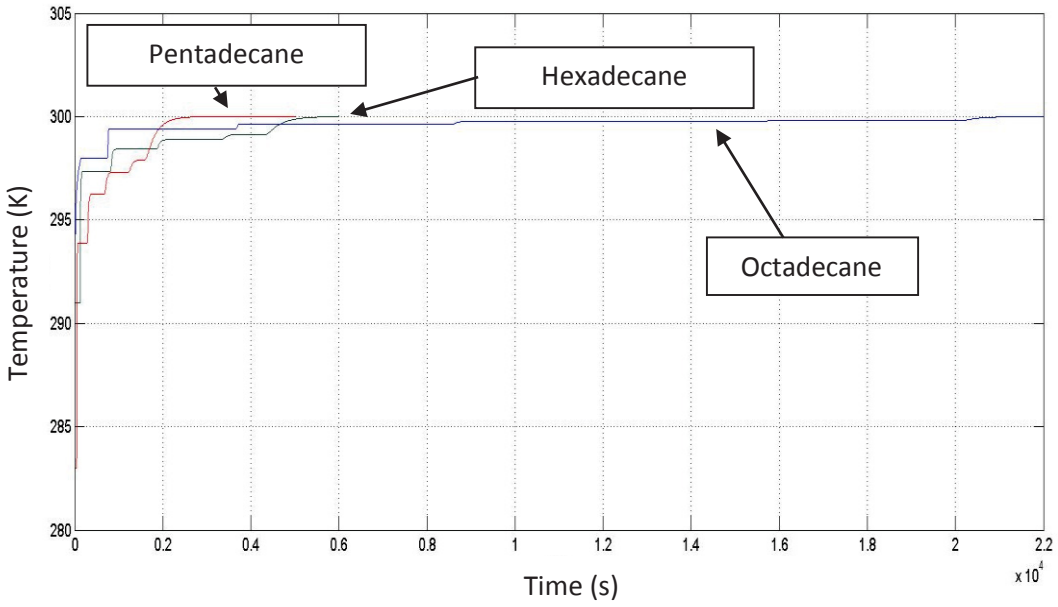

Figure 4.26 Temperature profile of a large volume TES cell for pentadecane, hexadecane, and octadecane

Table 4.13 Charge time for various phase change materials.

		Pentadecane	Hexadecane	Octadecane
Small Volume Charge Time	**s**	146	332.6	1295
Medium Volume Charge Time	**s**	620.9	1325	5187
Large Volume Charge Time	**s**	2490	5313	20700

As can be seen in Figures 4.24, 4.25, and 4.26 there are large differences in the temperature profiles and, thus, the charge times (see Table 4.13) for a TES cell designed with different PCMs. This can be attributed to a couple of different factors. The first of these is that the melting temperatures of the three materials are different. During the phase change from solid to liquid, the materials remain at a constant temperature which causes a temperature gradient between the working fluid and the PCM. As can be seen in the equations from Table 3.9, the heat rate into the PCM grows as the temperature difference between the working fluid and the PCM grows. Because of this, PCMs with a higher melting temperature, and therefore a smaller temperature difference with the working fluid during the phase change process experience a smaller heat rate than those with a lower melting temperature. This causes the phase change process for these materials to take longer, therefore, raising the charge time for a TES cell using these materials.

The second factor that influences the temperature profile and charge time for different materials is the differences in the latent heat of fusion for the different materials. The latent heat of fusion of a material is the amount of energy needed to complete a phase change for that material. Typical units are kJ/kg. A lower latent heat of fusion provides for a quicker phase change for a given heat rate, yet allows less energy to be stored during the phase change. Thus, lower latent heats of fusion give shorter charge times and lower heat storage values, while higher values give larger charge times and higher heat storage values. This in combination with the differences in melting temperature is why octadecane has a higher energy storage capacity than the other materials but also has the highest charging time out of the three. Because of these differences, it can be concluded that material selection is important to designing a TES cell for a PCES cell. For applications were a large charge time is undesirable, such as in a DEWS, materials must be selected that provide a large difference between their melting temperature and working fluid temperature as well as smaller latent heats of fusion. For applications were a longer charge time is desired, materials with melting temperatures close to the working fluid temperature as well as higher latent heats of fusion should be used.

It can also be seen in Table 4.13 that there is a large difference in the charge times for different volumes of the same phase change material. It can be seen that as the volume increases, the energy stored in the cell as well as the charge times also increase. Because of this, while larger TES cells can store more energy their charge time may prohibit their use on systems such as a DEWS where energy must be stored rapidly. In a system such as a DEWS, an array of smaller, and therefore faster charging TES cells with the same mass of PCM distributed between them may be more beneficial than a single, larger volume TES cell.

Chapter 5 - Conclusions and Recommendations

Several conclusions and recommendations are presented in this chapter. The conclusions are as follows

1. Microchannel heat exchangers can be used to reduce the mass needed for a TMS or allow a TMS's performance to increase for a given mass over current compact plate-fin heat exchanger technology.
2. For a microchannel or plate fin heat exchanger model, an assumption of 0.7 to 0.8 for the fin efficiency is a good one. This is beneficial as it reduces the number of optimization decision variables and decreases the solution time for sizing the heat exchangers.
3. Reducing the hydraulic diameter is a key factor in increasing the performance of compact and microchannel heat exchangers. Hydraulic diameter drives many different factors including the convective heat transfer rate, with lower values giving significantly better performance.
4. The mass flow rates, input temperatures, and heat loads imposed by the working fluids on a microchannel heat exchanger play a key part in the optimal dimensions needed to meet the heat transfer requirements.
5. For a phase change thermal energy storage cell, the material used as the PCM needs to be chosen based both on the charge time and the desired heat storage needed. When high heat transfer rates are needed, materials with lower melting temperatures and lower latent heats of fusion should be used. However, in order to get equivalent storage capacity to materials with higher melting temperatures and latent heats of fusion, cells made with these materials require more mass.
6. The volume used for a phase change thermal energy stored cell needs to be picked based on the application of the cell. For systems where rapid charging is needed, smaller volume cells will provide better performance than larger cells.

Recommendations made are as follows

1. The microchannel heat exchanger model designed here should be implemented in the tip-to-tail model used in Gvozdich[4] and Weise[6] and needed mass flow rates and temperatures of the working fluid to achieve the desired aircraft performance should be found. This

would increase the viability of the above results and give a better picture of the aircraft benefits of microchannel heat exchangers.

2. A non-gradient-based optimization method such as a genetic algorithm or particle swarm search should be implemented. The gradient based method used in this thesis research has trouble converging at certain heat loads and with a given set of design decision variables resulting in outliers to the data set. Implementing a non-gradient global optimization tool would help to alleviate some of these difficulties.
3. Improvements to the development and validation of the models presented here can be made. Experiments to generate more empirical data can be used to validate the heat exchanger models as well as provide better correlations for values such as the Nusselt number and friction factor in the microchannel heat exchanger. Better empirical data on the physical properties of the phase change materials in a composite foam would allow for a more accurate model to be generated.
4. Parallelization of the models in MATLAB could be conducted to decrease processing time.

Appendix A: Microchannel Heat Exchanger Sizing Algorithm

```
function [parameter] = HXsize_v12fixed(params,hbounds,mlneeded,fluids,params2,mat)
%HXsize(s1, h1, tf1, l1, t1, L, s2, h2, tf2, l2, t2) % %For Matlabs optimization
toolbox.
%This function written by Cody Reed and developed from code writtern by Peter Weise
%determines the weight and pressure drop of a microchannel or compact heat exchanger
%based on its physical parameters and heat transfer characteristics.  The methodology
used is laid out in the
%book "Compact Heat Exchangers: Selection, Design, and Operation" by J.E.
%Hesselgreaves.  Also see "Compact Heat Exchangers" by Kays and London.

%%% Heat exchanger fixed parameters:  The following parameters need to be
%%% fixed for a given optimization trial.  However, they can be varied.
%%% For example, the heat load varies from one heat exchanger to another.
%%% Additionally, the fluids vary from one exchanger to another.

s1 = params(1)/1000;        %
l1 = params(2)/1000;        %
tf1 = params(3)/1000;       %
t1 = params(4)/1000;        %
s2 = params(5)/1000;        %
l2 = params(6)/1000;        %
tf2 = params(7)/1000;       %
t2 = params(8)/1000;       %
L = params (9);       %

fluid1 = fluids.ctype;
fluid2 = fluids.htype;

m_dot1 = params2(1);      %(kg/s) flow rate
m_dot2 = params2(2);
T_in1 = params2(3);       %(K) inlet temperature. In the actual T2T model, the inlet
temperature will be based on downstream conditions and accepted as an input.
T_in2 = params2(4);       %(K) inlet temperature. See note above
Q_dot = params2(5);       %(kW) heat load

%% Material density,
material = mat;
%rho_m = (kg/m^3) material density
switch material
    case {'Stainless steel - 316'}
        rho_m = 8027;
        kfin = 15;
    case {'Aluminum'}
        rho_m = 2707;
        kfin = 210;
    case {'Copper'}
        rho_m = 8954;
        kfin = 400;
end

%%  Solves for the properties of each fluid based on inlet temperatures, steady state
outlet temperatures and fluid property correlations.
    [f1.cp, f1.rho, f1.k, f1.mu, f1.muT] = fluidproperties(fluid1);
    [f2.cp, f2.rho, f2.k, f2.mu, f2.muT] = fluidproperties(fluid2);

    %%% Specific heat
    cp1 = polyval(f1.cp,T_in1);
    cp2 = polyval(f2.cp,T_in2);

    %%% Density
```

```
    rho1 = polyval(f1.rho,T_in1);
    rho2 = polyval(f2.rho,T_in2);

    %%% Thermal Conductivity
    k1 = polyval(f1.k,T_in1);
    k2 = polyval(f2.k,T_in2);

    %%% Approximate outlet temperature
    T_out1 = T_in1 + Q_dot/(m_dot1*cp1);
    T_out2 = T_in2 - Q_dot/(m_dot2*cp2);

    %%% Dynamic Viscocity
    mu1 = interp1(f1.muT,f1.mu,(T_in1+T_out1)/2);
    mu2 = interp1(f2.muT,f2.mu,(T_in2+T_out2)/2);

    %%% Initialize Ac1 and Ac2.  Correct values will be solved for in an
    %%% iterative process.


    parameter.Ac1 = 0.01;
    parameter.Ac2 = 0.01;
    difference1 = inf;
    difference2= inf;
    count = 0;

    fzeroOptions = optimset('Display','off');
    %% This iterative while loop solves for Ac1 and Ac2.
    while count<=100 && abs(difference1)>=1e-5  && abs(difference2)>=1e-5
    % Using Fin Efficiency to determine fin length
        h1 = 10.6/1000;
        h2 = 10.6/1000;
        b1=h1+tf1;
        b2=h2+tf2;
        differenceh1=10000;
        differenceh2=10000;
        counth=1;
        while counth <=100 && abs(differenceh1)>1e-5 ||counth <=100 &&
abs(differenceh2)>1e-5
            parameter.dh1=(4*s1*h1*l1)/(2*(s1*l1+h1*l1+tf1*h1)+tf1*s1);
            parameter.dh2=(4*s2*h2*l2)/(2*(s2*l2+h2*l2+tf2*h2)+tf2*s2);

            sigma1=s1*(b1-tf1)/(s1+tf1)/(b1+t1);    %porosity of side 1
            sigma2=s2*(b2-tf2)/(s2+tf2)/(b2+t2);    %porosity of side 2

            alpha1=s1/h1;  %various aspect ratios used in calculating j and f
            delta1=tf1/l1;
            gamma1=tf1/s1;

            alpha2=s2/h2;
            delta2=tf2/l2;
            gamma2=tf2/s2;

            %%% parameter.Reynolds' number
            Re1=m_dot1*parameter.dh1/mu1/parameter.Ac1;
            Re2=m_dot2*parameter.dh2/mu2/parameter.Ac2;

            %%% Fanning friction factor
            parameter.f1=9.6243*(Re1^-0.7422)*(alpha1^-
0.1856)*(delta1^0.3053)*(gamma1^-0.2659)*((1+7.669E-
8*(Re1^4.429)*(alpha1^0.92)*(delta1^3.767)*(gamma1^0.236))^0.1);
            parameter.f2=9.6243*(Re2^-0.7422)*(alpha2^-
0.1856)*(delta2^0.3053)*(gamma2^-0.2659)*((1+7.669E-
8*(Re2^4.429)*(alpha2^0.92)*(delta2^3.767)*(gamma2^0.236))^0.1);
```

```
            %%% Colburn coefficient
            j1=0.6522*(Re1^-0.5403)*(alpha1^-0.1541)*(delta1^-0.1409)*(gamma1^-
0.0678)*((1+5.269E-5*(Re1^1.34)*(alpha1^0.504)*(delta1^0.456)*(gamma1^-1.055))^0.1);
            j2=0.6522*(Re2^-0.5403)*(alpha2^-0.1541)*(delta2^-0.1409)*(gamma2^-
0.0678)*((1+5.269E-5*(Re2^1.34)*(alpha2^0.504)*(delta2^0.456)*(gamma2^-1.055))^0.1);

                 %%% Nussult Number
            Pr1 = cp1*mu1/k1*1000;
            fd1 = 4*parameter.f1;
            if Re1 <2300
                aspectRatio = 2*s1/(2*h1);
                Nu1 =interp1([0 1/8,1/4,1/2,1], [8.235
2.904,4.35,3.017,3.091],aspectRatio);
            elseif Re1 >= 2300 && Re1 <= 5e4 && Pr1>=0.2 &&Pr1<=2000
                Nu1 = ((fd1/2)*(Re1-1000)*Pr1)/(1+12.7*(fd1/2)*(Pr1^(2/3)-1));
            elseif Re1 >= 10^4 && Re1 <= 5e5 && Pr1>=0.5 &&Pr1<=1.5
                Nu1 = 0.0214*(Re1^0.8-100)*Pr1^0.4*(1+(parameter.dh1/L)^(2/3));
            elseif Re1 >= 3e3 && Re1 <= 10^6 && Pr1>=0.5 &&Pr1<=500
                Nu1 = 0.012*(Re1^0.87-280)*Pr1^0.4*(1+(parameter.dh1/L)^(2/3));
            elseif Re1 >= 10^6 && Pr1>=0.6 &&Pr1<=160
                Nu1 = 0.023*Re1^(4/5)*Pr1^0.3;
            else
                error('Nussult Number not Defined for Given Reynolds Number or Prandtl
Number')
            end
            Pr2 = cp2*mu2/k2*1000;
            fd2 = 4*parameter.f2;
            if Re2 <2300
                aspectRatio = 2*s2/(2*h2);
                Nu2 =interp1([0 1/8,1/4,1/2,1], [8.235
2.904,4.35,3.017,3.091],aspectRatio);
            elseif Re2 >= 2300 && Re2 <= 5e4 && Pr2>=0.2 &&Pr2<=2000
                Nu2 = ((fd2/2)*(Re2-1000)*Pr2)/(1+12.7*(fd2/2)*(Pr2^(2/3)-
1))*(1+(parameter.dh2/L)^(2/3));
            elseif Re2 >= 10^4 && Re2 <= 5e5 && Pr2>=0.5 &&Pr2<=1.5
                Nu2 = 0.0214*(Re2^0.8-100)*Pr2^0.4*(1+(parameter.dh2/L)^(2/3));
            elseif Re2 >= 3e3 && Re2 <= 10^6 && Pr2>=1.5 &&Pr2<=500
                Nu2 = 0.012*(Re2^0.87-280)*Pr2^0.4*(1+(parameter.dh2/L)^(2/3));
            elseif Re2 >= 10^6 && Pr2>=0.6 &&Pr2<=160
                Nu2 = 0.023*Re2^(4/5)*Pr2^0.3;
            else
                error('Nussult Number not Defined for Given Reynolds Number or Prandtl
Number')
            end
            convh1 = Nu1*k1/parameter.dh1;
            convh2 = Nu2*k2/parameter.dh2;
            m1eff = (2*convh1/(kfin*tf1)*(1+tf1/l1))^(1/2);
            m2eff = (2*convh2/(kfin*tf2)*(1+tf2/l2))^(1/2);
            l1needed = m1needed/m1eff;
            l2needed = m1needed/m2eff;
            h1new = (l1needed+tf1)*2;
            h2new = (l2needed+tf2)*2;
            differenceh1 = h1new-h1;
            differenceh2 = h2new-h2;
            h1 = h1new;
            h2 = h2new;
            counth=counth+1;
        end
        %Using the converged fin length to determine a new estimate for Ac
        b1=h1+tf1;
        b2=h2+tf2;
```

```
        parameter.dh1=(4*s1*h1*l1)/(2*(s1*l1+h1*l1+tf1*h1)+tf1*s1);
        parameter.dh2=(4*s2*h2*l2)/(2*(s2*l2+h2*l2+tf2*h2)+tf2*s2);

        sigma1=s1*(b1-tf1)/(s1+tf1)/(b1+t1);    %porosity of side 1
        sigma2=s2*(b2-tf2)/(s2+tf2)/(b2+t2);    %porosity of side 2

        alpha1=s1/h1;  %various aspect ratios used in calculating j and f
        delta1=tf1/l1;
        gamma1=tf1/s1;

        alpha2=s2/h2;
        delta2=tf2/l2;
        gamma2=tf2/s2;



        %%% parameter.Reynolds' number
        Re1=m_dot1*parameter.dh1/mu1/parameter.Ac1;
        Re2=m_dot2*parameter.dh2/mu2/parameter.Ac2;

        %%% Fanning friction factor
        parameter.f1=9.6243*(Re1^-0.7422)*(alpha1^-0.1856)*(delta1^0.3053)*(gamma1^-
0.2659)*((1+7.669E-8*(Re1^4.429)*(alpha1^0.92)*(delta1^3.767)*(gamma1^0.236))^0.1);
        parameter.f2=9.6243*(Re2^-0.7422)*(alpha2^-0.1856)*(delta2^0.3053)*(gamma2^-
0.2659)*((1+7.669E-8*(Re2^4.429)*(alpha2^0.92)*(delta2^3.767)*(gamma2^0.236))^0.1);

        %%% Colburn coefficient
        j1=0.6522*(Re1^-0.5403)*(alpha1^-0.1541)*(delta1^-0.1409)*(gamma1^-
0.0678)*((1+5.269E-5*(Re1^1.34)*(alpha1^0.504)*(delta1^0.456)*(gamma1^-1.055))^0.1);
        j2=0.6522*(Re2^-0.5403)*(alpha2^-0.1541)*(delta2^-0.1409)*(gamma2^-
0.0678)*((1+5.269E-5*(Re2^1.34)*(alpha2^0.504)*(delta2^0.456)*(gamma2^-1.055))^0.1);

                %%% Nussult Number
        Pr1 = cp1*mu1/k1*1000;
        fd1 = 4*parameter.f1;
        if Re1 <2300
            aspectRatio = 2*s1/(2*h1);
            Nu1 =interp1([0 1/8,1/4,1/2,1], [8.235
2.904,4.35,3.017,3.091],aspectRatio);
        elseif Re1 >= 2300 && Re1 <= 5e4 && Pr1>=0.2 &&Pr1<=2000
            Nu1 = ((fd1/2)*(Re1-1000)*Pr1)/(1+12.7*(fd1/2)*(Pr1^(2/3)-1));
        elseif Re1 >= 10^4 && Re1 <= 5e5 && Pr1>=0.5 &&Pr1<=1.5
            Nu1 = 0.0214*(Re1^0.8-100)*Pr1^0.4*(1+(parameter.dh1/L)^(2/3));
        elseif Re1 >= 3e3 && Re1 <= 10^6 && Pr1>=0.5 &&Pr1<=500
            Nu1 = 0.012*(Re1^0.87-280)*Pr1^0.4*(1+(parameter.dh1/L)^(2/3));
        elseif Re1 >= 10^6 && Pr1>=0.6 &&Pr1<=160
            Nu1 = 0.023*Re1^(4/5)*Pr1^0.3;
        else
            error('Nussult Number not Defined for Given Reynolds Number or Prandtl
Number')
        end
        Pr2 = cp2*mu2/k2*1000;
        fd2 = 4*parameter.f2;
        if Re2 <2300
            aspectRatio = 2*s2/(2*h2);
            Nu2 =interp1([0 1/8,1/4,1/2,1], [8.235,
2.904,4.35,3.017,3.091],aspectRatio);
        elseif Re2 >= 2300 && Re2 <= 5e4 && Pr2>=0.2 &&Pr2<=2000
            Nu2 = ((fd2/2)*(Re2-1000)*Pr2)/(1+12.7*(fd2/2)*(Pr2^(2/3)-
1))*(1+(parameter.dh2/L)^(2/3));
        elseif Re2 >= 10^4 && Re2 <= 5e5 && Pr2>=0.5 &&Pr2<=1.5
            Nu2 = 0.0214*(Re2^0.8-100)*Pr2^0.4*(1+(parameter.dh2/L)^(2/3));
        elseif Re2 >= 3e3 && Re2 <= 10^6 && Pr2>=1.5 &&Pr2<=500
```

```
            Nu2 = 0.012*(Re2^0.87-280)*Pr2^0.4*(1+(parameter.dh2/L)^(2/3));
        elseif Re2 >= 10^6 && Pr2>=0.6 &&Pr2<=160
            Nu2 = 0.023*Re2^(4/5)*Pr2^0.3;
        else
            error('Nussult Number not Defined for Given Reynolds Number or Prandtl
Number')
        end
        convh1 = Nu1*k1/parameter.dh1;
        convh2 = Nu2*k2/parameter.dh2;
        m1eff = (2*convh1/(kfin*tf1)*(1+tf1/l1))^(1/2);
        m2eff = (2*convh2/(kfin*tf2)*(1+tf2/l2))^(1/2);
        l1eff = h1/2-tf1;
        l2eff = h2/2-tf2;
        eta1 = tanh(m1eff*l1eff)/(m1eff*l1eff);
        eta2 = tanh(m2eff*l2eff)/(m2eff*l2eff);

        %%% Effectiveness-Ntu method
        T_h1=max(T_in1,T_in2);
        T_c1=min(T_in1,T_in2);
        Cmax=max(m_dot1*cp1,m_dot2*cp2);
        Cmin=min(m_dot1*cp1,m_dot2*cp2);
        Cstar=Cmin/Cmax;
        epsilon = Q_dot/(Cmin*(T_h1-T_c1));
        %if 0>=epsilon || epsilon >1
            %disp('epsilon must be between 0 and 1. Heat load (Q_dot) is too large or
T_h1-T_c1 is too small')
            %break
        %end

        if (0.99<=Cstar)&&(Cstar<=1.01)
            Ntu=epsilon/(1-epsilon);
        else
            Ntu=log((epsilon-1)/(Cstar*epsilon-1))/(Cstar-1);
        end

        N1=2*Ntu/eta1;
        N2=2*Ntu/eta2;

        %%% Pressure drop

parameter.del_P1=((m_dot1/parameter.Ac1)^2)*4*L*parameter.f1/2/rho1/parameter.dh1;

parameter.del_P2=((m_dot2/parameter.Ac2)^2)*4*L*parameter.f2/2/rho2/parameter.dh2;

        %%% Prandtl number
        Pr1=cp1*mu1/k1*1000;
        Pr2=cp2*mu2/k2*1000;

        %%% Flow velocity
        G1=sqrt(2*rho1*parameter.del_P1*j1/parameter.f1/(Pr1^(2/3))/N1);
        G2=sqrt(2*rho2*parameter.del_P2*j2/parameter.f2/(Pr2^(2/3))/N2);

        %%% Flow area
        Ac1_0=m_dot1/G1;
        Ac2_0=m_dot2/G2;

        Ac1Last = parameter.Ac1;
        Ac2Last = parameter.Ac2;

        difference1=parameter.Ac1-Ac1_0;
        difference2=parameter.Ac2-Ac2_0;

        parameter.Ac1=Ac1_0;
```

```
        parameter.Ac2=Ac2_0;

        count = count + 1;
    end

    parameter.Ac1=Ac1Last;
    parameter.Ac2=Ac2Last;
   %disp('iterations =')
   %disp(count)
%%% Calculate volume and Weight
    parameter.weight_kg=rho_m*L*(parameter.Ac1/sigma1*(1-
sigma1)+parameter.Ac2/sigma2*(1-sigma2));
    parameter.weight_f1 = (parameter.Ac1*rho1*L);
    parameter.weight_f2 = parameter.Ac2*rho2*L;
    parameter.vol_HX = L*(parameter.Ac1/sigma1*(1-sigma1)+parameter.Ac2/sigma2*(1-
sigma2));
    parameter.vol_f = (parameter.Ac1+parameter.Ac2)*L;
    Beta = [4*sigma1/parameter.dh1 4*sigma2/parameter.dh2];
    parameter.vol1 = L*parameter.Ac1;
    parameter.vol2 = L*parameter.Ac2;
    parameter.As1 =Beta(1) * (L*(parameter.Ac1/sigma1*(1-sigma1)) + parameter.Ac1);
    parameter.As2 =Beta(2) * (L*(parameter.Ac2/sigma2*(1-sigma2)) + parameter.Ac2);
    parameter.L = L;

%%% Additional outputs,
    parameter.ratios1 = [alpha1 delta1 gamma1];
    parameter.ratios2 = [alpha2 delta2 gamma2];
    parameter.Achx = (sqrt(parameter.Ac1) + sqrt(parameter.Ac2))/2*parameter.L;
    parameter.Aht1 = parameter.Ac1*(s1 + tf1)/(s1*h1)*L;
    parameter.Aht2 = parameter.Ac2*(s2 + tf2)/(s2*h2)*L;
```

References

1. von Spakovsky, M.R. "Mission and Aircraft level Thermal Management System Research Overview". in *Aerospace Systems & Technology Conference*. 2014. Cincinnati, OH.
2. Clare, J., *Examples of More Electric Aircraft Research in the Aerospace Research Centre*.
3. "Directed Energy Weapons", D.o. Defense, Editor. 2007, Office of the Under Secretary of Defense.
4. Gvozdich, G., "Modeling the Effects of Transient High Energy Weapon Subsystems on High-performance Aerospace Systems, in Mechanical Engineering". 2011, M.S. thesis advisor: M.R. von Spakovsky, ME dept., Virginia Tech Blacksburg, VA.
5. Weise, P., "Mission-Integrated Synthesis/Design Optimization of Aerospace Systems under Transient Conditions", in *Mechanical Engineering*. 2012, M.S. thesis advisor: M.R. von Spakovsky, ME dept., Virginia Tech: Blacksburg, VA.
6. Weise, P., G. Gvozdich, and M.R. von Spakovsky. "INVENT: Mission-Integrated Optimization of a Tip-to-Tail High Performance Aircraft System". in *50th AIAA Aerospace Sciences Meeting, Nashville, TN*. 2012.
7. Raj, P., "Airplane Design Process". 2014: Virginia Tech.
8. "Cost of Design Process Change". Defense Systems Management College.
9. Allison, D.L., "Multidisciplinary Analysis and Design Optimization of an Efficient Supersonic Air Vehicle". 2013, Virginia Polytechnic Institute and State University.
10. Adam Maser, E.G., Dimitri Mavris, "Thermal Management Modeling for Integrated Power Systems in a Transient, Multidisciplinary Environment", in *AIAA/ASME/SAE/ASEE Joint Propulsion Conference & Exhibit*. 2009: Denver, CO.
11. Blanding, D., "Subsystem Design and Integration for the More Electric Aircraft, in 25th International Congress of the Aeronautical Sciences". 2006.
12. Jeffrey Freeman, P.O., Michael Green, Andrew Gibson, Benjamin Schiltgen, "Challenges and opportunities for electric aircraft thermal management". Aircraft Engineering and Aerospace Technology: An International Journal, 2014. **86**(6): p. 519-524.
13. Gulczinski, F., "Integrated Vehicle Energy Technology Overview", D.o. Defense, Editor. 2012, Air Force Research Lab.
14. Bodie, M., et al., *Thermal analysis of an integrated aircraft model.* AIAA Paper, 2010. **20**: p. 0-288.
15. Hesselgreaves, J.E., *Compact heat exchangers: selection, design and operation*. 2001: Gulf Professional Publishing.
16. "Finned Tube versus Plate Fin Heat Exchanger". 2015. http://fchart.com/ees/heat_transfer_library/compact_hx/hs100.htm
17. Kays, W.M. and A.L. London, *Compact heat exchangers.* 1984.
18. Shah, R.K. and D.P. Sekulic, *Fundamentals of heat exchanger design*. 2003: John Wiley & Sons.
19. Mathew, B. and H. Hegab. "Performance evaluation of parallel flow microchannel heat exchanger subjected to external heat transfer". in *ASME 2007 International Mechanical Engineering Congress and Exposition*. 2007. American Society of Mechanical Engineers.
20. Williams, M., et al., "Advanced heat exchanger technology for aerospace applications". 2008, SAE Technical Paper. 64

21. Ashman, S. and S.G. Kandlikar. "A review of manufacturing processes for microchannel heat exchanger fabrication. in ASME 4th International Conference on Nanochannels, Microchannels, and Minichannels". 2006. American Society of Mechanical Engineers.
22. Shanmugasundaram, V., M. Ramalingam, and B. Donovan, "Power and Thermal Technologies for Aerospace Applications″. AFRL, Interim Report AFRL-PR-WP-TR-2007-2068, Wright-Patterson AFB, OH, 2007.
23. Shanmugasundaram, V., et al. "Aircraft Based Pulsed Power System Thermal Management Options With Energy Storage". in *4th International Energy Conversion Engineering Conference, San Diego, California*. 2006.
24. Warren M. Rohsenow, J.P.H., E.N. Ganic, *Handbook of heat transfer applications*. 1985, McGraw-Hill, New York.
25. Gnielinski, V., A. Zukaukas, and A. Skrinska, *Heat exchanger design handbook.* Sec, 1983.
26. Jiang, P.-X., et al., "Thermal–hydraulic performance of small scale micro-channel and porous-media heat-exchangers". International Journal of Heat and Mass Transfer, 2001. **44**(5): p. 1039-1051.